4-26-2019

PBRM1 Regulates Stress Response in Epithelial Cells

Elizabeth G. Porter

Alisha Dhiman

Basudev Chowdhury

Benjamin C. Carter

Hang Lin

See next page for additional authors

Authors

Elizabeth G. Porter, Alisha Dhiman, Basudev Chowdhury, Benjamin C. Carter, Hang Lin, Jane C. Stewart, Majid Kazemian, Michael K. Wendt, and Emily C. Dykhuizen

iScience

CellPress

Article

PBRM1 Regulates Stress Response in Epithelial Cells

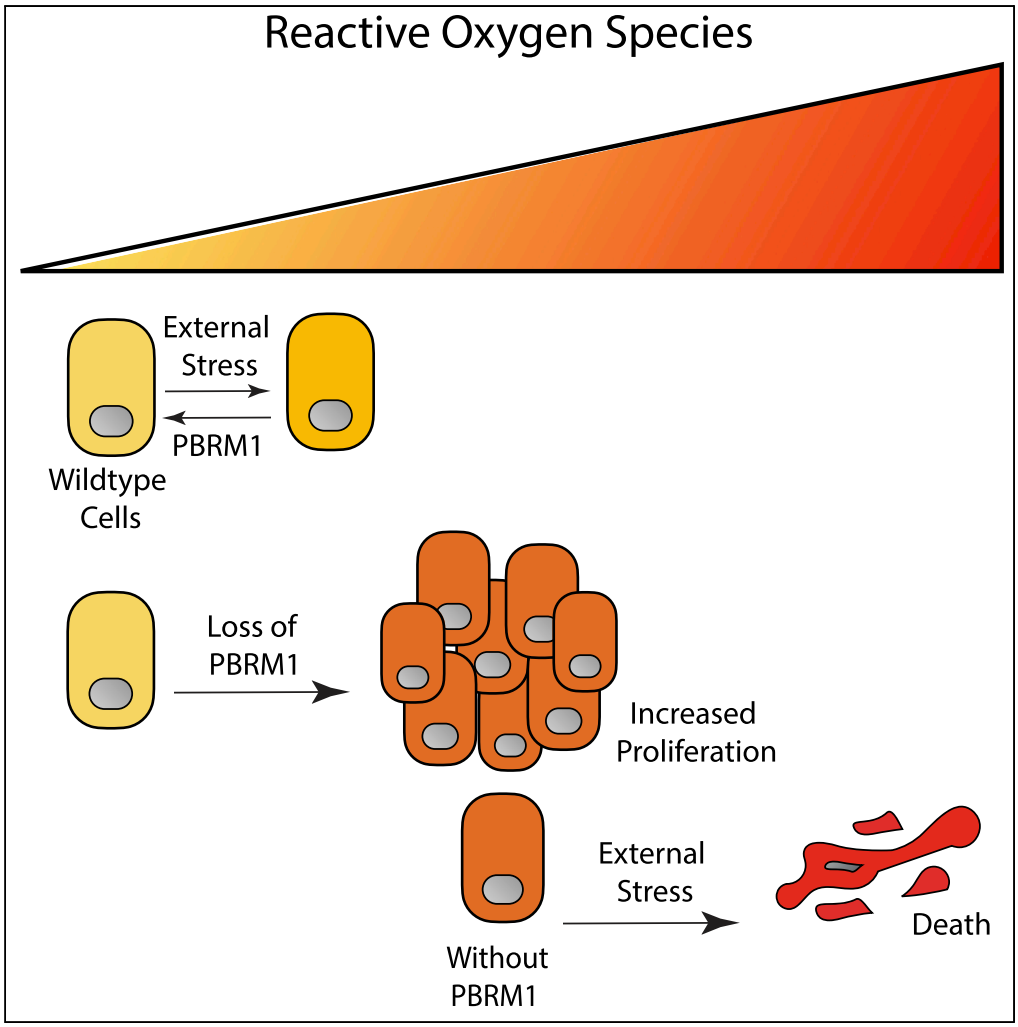

Elizabeth G. Porter, Alisha Dhiman, Basudev Chowdhury, ..., Majid Kazemian, Michael K. Wendt, Emily C. Dykhuizen

edykhui@purdue.edu

HIGHLIGHTS

PBRM1 facilitates the expression of stress response genes in epithelial cells

Deletion of PBRM1 promotes growth under low-stress conditions

PBRM1 restrains ROS generation and induces apoptosis under high-stress conditions

Under H_2O_2 stress, PBRM1 cooperates with cJun and NRF2 to induce gene expression

Porter et al., iScience *15*, 196–210
May 31, 2019
https://doi.org/10.1016/j.isci.2019.04.027

iScience

CellPress

Article

PBRM1 Regulates Stress Response in Epithelial Cells

Elizabeth G. Porter,[1,3] Alisha Dhiman,[1,3] Basudev Chowdhury,[1] Benjamin C. Carter,[1] Hang Lin,[1] Jane C. Stewart,[1] Majid Kazemian,[2] Michael K. Wendt,[1] and Emily C. Dykhuizen[1,4,*]

SUMMARY

Polybromo1 (PBRM1) is a chromatin remodeler subunit highly mutated in cancer, particularly clear cell renal carcinoma. PBRM1 is a member of the SWI/SNF subcomplex, PBAF (PBRM1-Brg1/Brm-associated factors), and is characterized by six tandem bromodomains. Here we establish a role for PBRM1 in epithelial cell maintenance through the expression of genes involved in cell adhesion, metabolism, stress response, and apoptosis. In support of a general role for PBRM1 in stress response and apoptosis, we observe that loss of PBRM1 results in an increase in reactive oxygen species generation and a decrease in cellular viability under stress conditions. We find that loss of PBRM1 promotes cell growth under favorable conditions but is required for cell survival under conditions of cellular stress.

INTRODUCTION

PBRM1, a gene that encodes a subunit of the PBRM1-Brg1/Brm-associated factors (PBAF) chromatin remodeling complex, is mutated in over 3% of all cancers with the highest mutation rate occurring in clear cell renal cell carcinoma (ccRCC), where it is mutated in 40%–50% of patients (Cancer Genome Atlas Research Network, 2013; Peña-Llopis et al., 2012; Varela et al., 2011). The PBAF chromatin remodeling complex is a minor subcomplex of the human SWI/SNF, or BAF, chromatin remodeling family, subunits of which (*SMARCA4* [BRG1], *ARID1A*, and *SMARCB1* [SNF5 or BAF47]) are also frequently mutated in cancers (Kadoch et al., 2013; Shain and Pollack, 2013). Along with PBRM1, the PBAF subcomplex exclusively contains ARID2, BRD7, BAF45A, as well as several subunits shared with the more abundant BAF complex (Kaeser et al., 2008; Tatarskiy et al., 2017; Xue et al., 2000). PBRM1 is composed of several domains associated with binding to chromatin including six tandem bromodomains (BDs), two bromo-adjacent homology domains, and a high-mobility group, implicating PBRM1 as a chromatin-targeting subunit of PBAF. For the most part, the chromatin signatures bound by PBRM1 have not yet been determined, although histone 3 lysine 14 acetylation (H3K14Ac) has been defined as a primary target for the second bromodomain (BD2) *in vitro* (Charlop-Powers et al., 2010), and validated as the acetylation mark most critical for association of the full PBAF complex to histone peptides (Porter and Dykhuizen, 2017). PBRM1 has homology to RSC1, RSC2, and RSC4 subunits of the yeast RSC chromatin remodeling complex, which also interacts with H3K14Ac, particularly during DNA damage (Duan and Smerdon, 2014; Wang et al., 2012). However, unlike subunits of RSC, PBRM1 does not seem to be necessary for viability in the majority of mammalian cell types, and in fact, although PBRM1 is essential for embryonic heart development in mice (Huang et al., 2008; Wang et al., 2004), adult mice with knockout of PBRM1 are phenotypically normal except for an age-related hematopoietic stem cell defect (Lee et al., 2016).

The most well-defined cellular role for PBRM1 is in DNA damage repair (Brownlee et al., 2014; Kakarougkas et al., 2014), which is in line with observation of H3K14Ac at sites of DNA damage (Lee et al., 2010); however, the low mutational burden and relative genome stability of PBRM1-mutant tumors makes it unclear how this role in DNA damage repair relates to the tumor-suppressive phenotypes of PBRM1 (Sato et al., 2013). As such, most of the focus has been on deciphering how transcriptional functions for PBRM1 relate to a role in tumor suppression. Transcriptional profiling of human ccRCC indicates that PBRM1 mutant tumors have a hypoxic transcriptional signature (Sato et al., 2013), which is in agreement with recent reports that mutation of PBRM1 amplifies the hypoxia-inducible factor (HIF) transcriptional program signature induced upon von Hippel-Lindau (VHL) deletion in cell culture (Gao et al., 2017) and in a mouse renal cancer model (Nargund et al., 2017). Recent work with kidney-specific (KSP and PAX8) Cre mouse models indicates that VHL knockout or PBRM1 knockout alone is not sufficient for cancer formation but that both are required for kidney tumor formation in mice (Espana-Agusti et al., 2017; Gu et al., 2017; Nargund et al., 2017).

[1]Department of Medicinal Chemistry and Molecular Pharmacology, Purdue University, West Lafayette, IN 47906, USA

[2]Department of Biochemistry, Purdue University, West Lafayette, IN 47906, USA

[3]These authors contributed equally

[4]Lead Contact

*Correspondence: edykhui@purdue.edu

https://doi.org/10.1016/j.isci.2019.04.027

Although these recent mouse studies have solidified a role for PBRM1 as a bona fide tumor suppressor in renal cancer, the molecular mechanism by which PBRM1 acts as a tumor suppressor is still unclear. For example, PBRM1 exhibits tumor-suppressive phenotypes in a subset of cancer cell lines (Chowdhury et al., 2016; Huang et al., 2015; Xia et al., 2008), but PBRM1 knockdown in many cell lines produces no phenotype (Chowdhury et al., 2016; Gao et al., 2017) or even decreases cellular viability (Lee et al., 2016). In the renal cancer setting, this context-specific function is mediated, in part, through HIF1a expression, which is required for PBRM1's tumor suppressor phenotype in renal cell lines (Murakami et al., 2017) (Shen et al., 2011); however, the context-dependent function observed in other cell types is still undefined. Here we used epithelial cell lines to define how the function of PBRM1 in non-transformed cells may relate to its function as a tumor suppressor. Through genome-wide transcriptional analysis, we have defined a general role for PBRM1 in regulating the expression of genes involved in stress response, particularly endoplasmic reticulum (ER) stress and apoptosis. To support this general function, we have found that loss of PBRM1 results in accumulation of reactive oxygen species (ROS) and a failure to induce apoptosis under a variety of high-stress conditions. Based on our findings, we propose that PBRM1 acts to regulate stress response genes that restrain cellular proliferation under low-stress conditions but protect cells under high-stress conditions.

RESULTS

Knockdown of PBRM1 in Epithelial Cells Promotes Growth and a Loss of Epithelial Cell Maintenance

As mutation of PBRM1 in epithelial cells is an early event in tumorigenesis (Gerlinger et al., 2014) we set out to understand the tumor-suppressive role PBRM1 plays in various cell models of epithelium. We depleted *PBRM1* using lentiviral short hairpin RNA (shRNA) in several epithelial cell lines including the immortalized human kidney epithelial cell line HK-2, the canine kidney epithelial cell line MDCK, and the mouse mammary epithelial cell line NMuMG (Figure S1A). In addition to its role in renal cancer, PBRM1 acts as a tumor suppressor in mammary-epithelium-derived cancers as observed in PBRM1-mutated (Xia et al., 2008) and PBRM1-downregulated breast cancers (Figure S1B) (Mo et al., 2015). The loss of PBRM1 resulted in an increase in proliferation in all of these cell lines (Figure 1A). As NMuMG is the most commonly used cell model of epithelial differentiation, we used it for further analysis and validated the PBRM1 knockdown phenotype using CRISPR-mediated knockout of PBRM1 (Figures 1A and S1C). In NMuMG cells, knockdown of PBRM1 decreases protein levels of E-cadherin, a marker of epithelial cells, and increases vimentin, a marker of mesenchymal cells (Figure 1B) (Kalluri and Weinberg, 2009). A decrease in E-cadherin at adherens junctions results in a weakening of cell-cell adhesion and also results in the release of bound β-catenin, which normally anchors E-cadherin to the actin cytoskeleton (Kalluri and Weinberg, 2009). In agreement with this, we observed an increase in nuclear β-catenin signaling upon PBRM1 knockdown (Figure 1C). The complete loss of E-cadherin expression and cellular morphology characteristic of a robust epithelial-to-mesenchymal transition (EMT) was not observed; instead, the observed phenotypes reflect a partial EMT or a reduction in epithelial maintenance. The same phenotypes were also observed upon knockdown of BRD7, another PBAF-specific subunit (Kaeser et al., 2008), although these findings are complicated by a decrease in PBRM1 upon BRD7 knockdown (Figure S1D). Consistent with the documented role for the BAF complex in maintaining human mammary epithelial proliferation (Cohet et al., 2010), knockdown of BAF subunits ARID1A or BRG1 resulted in cell arrest and death (data not shown).

A decrease in E-cadherin in epithelial cells during EMT results in a weakening of cell-cell contacts, resulting in an increase in migration rates, which was observed in the PBRM1 knockdown (Figure 1D) and PBRM1 knockout (Figure S1E). A decrease in E-cadherin also results in a decrease in cellular polarity, a feature central to epithelial function. To investigate the contribution of PBRM1 to the maintenance of epithelial cell polarity we plated NMuMG cells in Matrigel-based 3D culture where they self-assemble into luminal structures consisting of hollow acini displaying apical-basal polarity (Hall et al., 1982). Upon PBRM1 knockdown, the spheres fail to establish hollow lumen and lose both ZO-1 at apical tight junctions and basal or lateral staining of alpha 6 integrin (Figures 1E and S1F). This phenotype is consistent with that observed in NMuMG epithelial cells with PTEN deletion or PI3K-activating mutation (Berglund et al., 2012).

PBRM1 Regulates Genes Involved in Cell Adhesion, Signaling, Stress Response, and Apoptosis

To identify genes regulated by PBRM1 in epithelial cells, we performed RNA sequencing (RNA-seq) from control and PBRM1 knockdown NMuMG cells. In total, we identified 2,467 genes with significantly

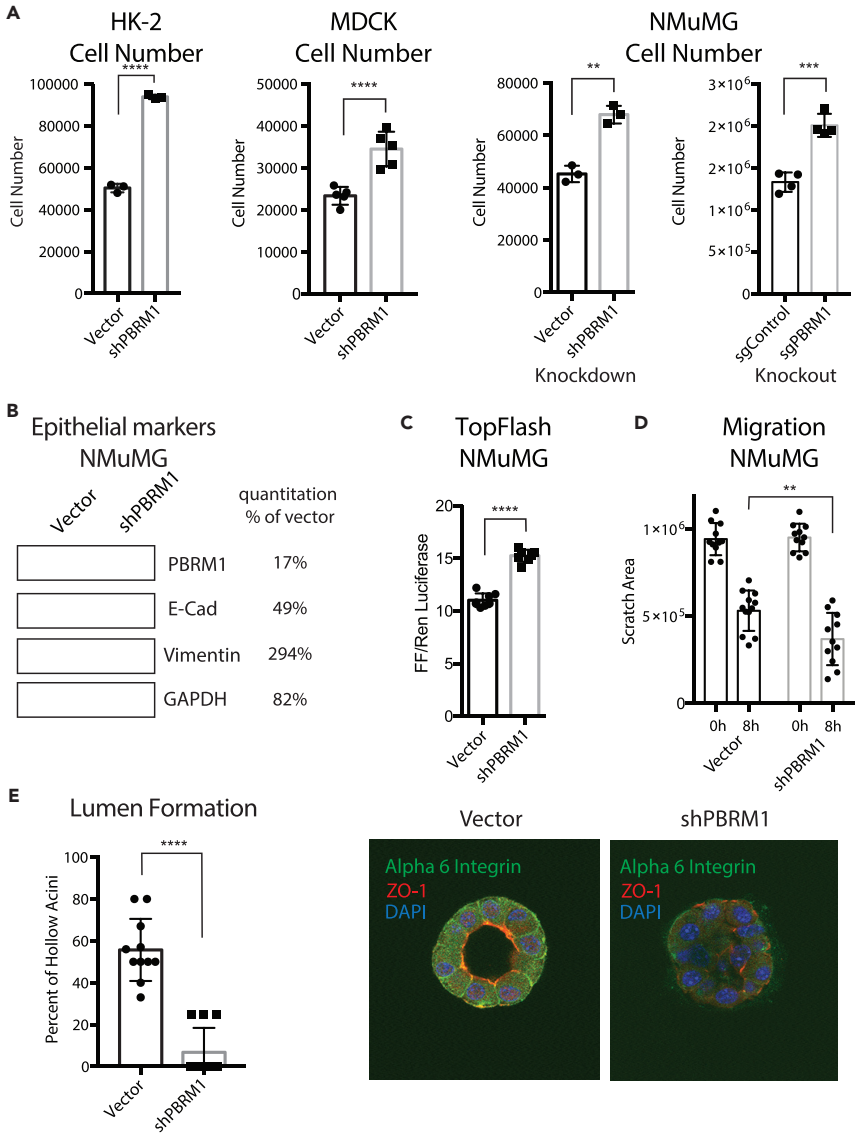

Figure 1. Knockdown of PBRM1 in Cell Line Models of Epithelial Differentiation Promotes Growth and a Loss of Epithelial Cell Maintenance

(A) Epithelial cell lines HK-2 (human kidney), MDCK (canine kidney), and NMuMG (mouse mammary), were counted after 72 h growth, and cell number are presented as mean ± SD. n = 3–5.

(B) Immunoblot analysis of whole-cell lysates from NMuMG cells indicates that PBRM1 knockdown results in decreased E-cadherin and increased vimentin expression. Quantification represented as percent of shPBRM1 over vector.

(C) β-Catenin signaling, as measured using TopFlash reporter assay in NMuMG cells with vector control or shPBRM1. Individual replicates are presented as mean ± SD, n = 8.

(D) Migration differences determined by measuring the cell-free area at 40× magnification at 0 and 8 h after scratching with standard pipette tip. The data from 12 independent images were statistically analyzed and presented as mean ± SD, n = 12.

(E) Acini with hollow lumen from NMuMG cells grown in 3D culture for 10 days were counted in a blinded manner, and the frequency was calculated from total acini in a field of image (average of 5–6 acini per field). The data from 11 independent images were statistically analyzed (Student's t test) and presented as mean ± SD, n = 11. Representative image of acini grown for 14 days were analyzed using immunofluorescence staining with anti-ZO1 (red) and anti-alpha-6-integrin (green). Nuclei (blue) were visualized by DAPI.

**p < 0.01, ***p < 0.001, ****p < 0.0001 (paired Student's t test). ns, not significant. Error bars represent SD. Also see Figure S1.

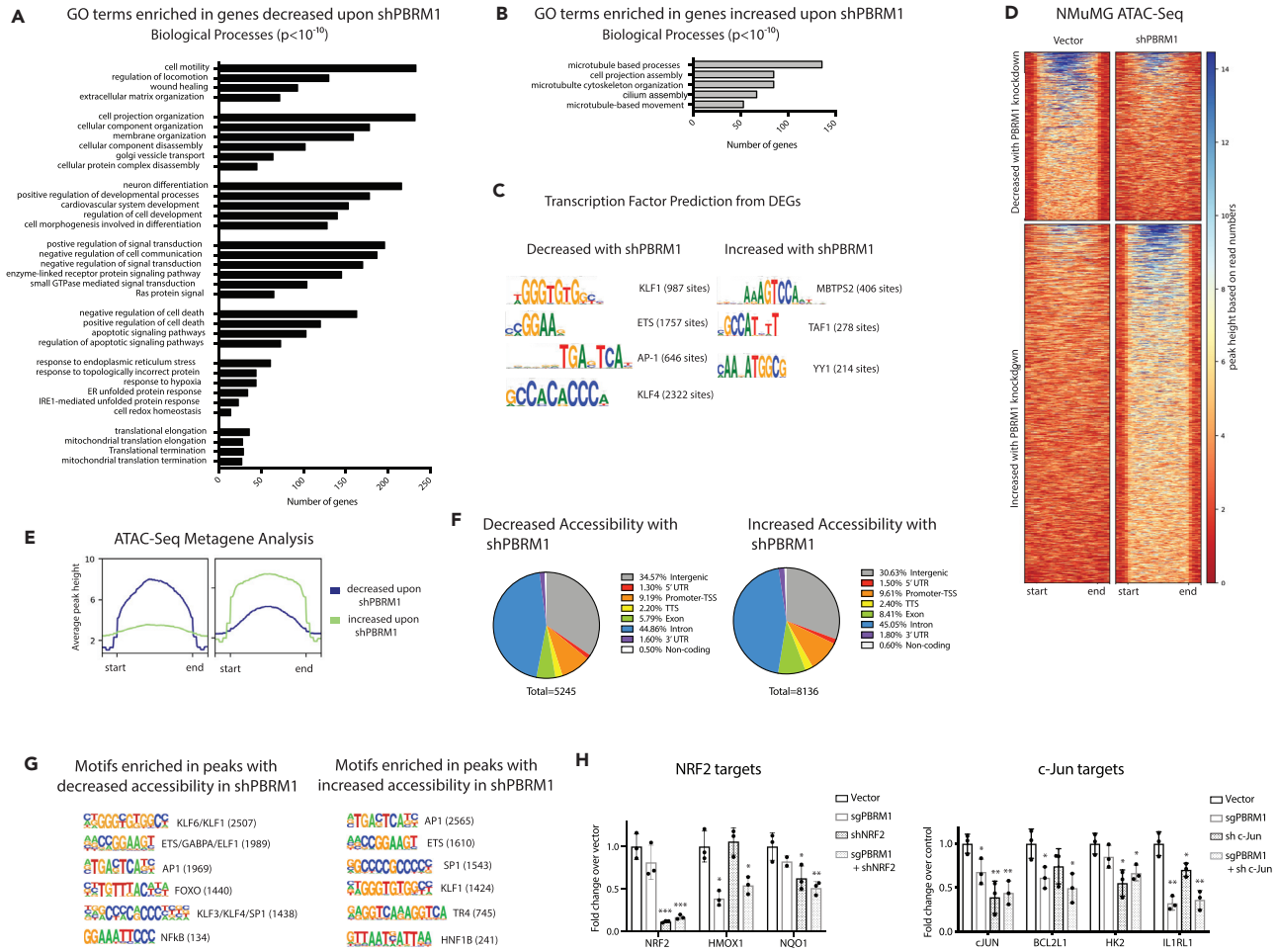

Figure 2. PBRM1 Regulates Genes Involved in Cell Adhesion, Signaling, Stress Response, and Apoptosis and Is Predicted to Cooperate with Transcription Factors Involved in Response to Stress

(A) Top overrepresented biological process GO terms (p values < 10^{-10}) for differentially expressed genes that are downregulated in NMuMG cells with shPBRM1.

(B) Top overrepresented biological process GO terms (p values < 10^{-10}) for differentially expressed genes that are upregulated in NMuMG cells with shPBRM1.

(C) Putative transcription factors were identified for genes exhibiting differential expression in NMuMG cells with shPBRM1.

(D) Heatmaps of regions identified as differentially accessible with PBRM1 knockdown using ATAC-seq analysis of NMuMG cells. Regions of at least 1.5-fold differential accessibility were calculated between pooled samples of three biological replicates.

(E) Metagene plots of the regions identified as differentially accessible with PBRM1 knockdown using ATAC-seq analysis of NMuMG cells.

(F) Genomic elements associated with the differentially accessible peaks. The overall distribution was calculated as a percentage of the total differentially accessible regions for each condition.

(G) Motif analysis was performed using HOMER for the differentially accessible peaks. Statistically significant motifs were identified based on relative enrichment over genomic areas with similar AT content.

(H) The contribution of PBRM1 to the transcriptional regulation of NRF2 (left) or c-Jun (right) target genes using qRT-PCR and *OAZ1* as the housekeeping gene. n = 3. *p < 0.05, **p < 0.01, ***p < 0.001 (paired Student's t test). Error bars represent SD.

Also see Figure S2 and Table S1.

increased transcript levels and 1,927 genes with significantly decreased transcript levels upon *PBRM1* knockdown (Table S1). Gene ontology (GO) analysis identified numerous pathways significantly enriched in genes downregulated upon shPBRM1, including cell movement, cell structure, development, and signaling (Figure 2A), as would be expected based on the loss of epithelial characteristics in the PBRM1 knockdown (Figure 1). In addition, there were numerous enriched biological pathways involved in stress response, cellular homeostasis, translational elongation, and apoptosis. In contrast, there were few

significantly enriched biological pathways for genes upregulated upon PBRM1 knockdown; however, these pathways included microtubule-based processes (Figure 2B).

PBRM1 Is Predicted to Cooperate with Transcription Factors that Facilitate the Response to Stress

We further utilized the RNA-seq datasets to predict upstream regulators that might cooperate with PBRM1 in the transcription of target genes. For genes decreased with shPBRM1, several enriched consensus sequences were identified, with the most robust identified for KLF transcription factors (TFs), including KLF4 (Figure 2C), which is required for epithelial cell homeostasis (Ghaleb et al., 2011; Yu et al., 2012). In fact, the KLF4 knockdown in NMuMG cells has a similar phenotype to the PBRM1 knockdown (Tiwari et al., 2013). In addition, there was significant enrichment for genes with consensus sequences for ETS TFs, which are primarily thought of as oncogenic, but are involved in a variety of processes like cell cycle, differentiation, and apoptosis (Sizemore et al., 2017). Last, there was significant enrichment for genes with consensus sequences for AP-1 TFs, such as JUN/FOS and NRF2, which are upregulated during stress (Jiang et al., 2016; Rössler and Thiel, 2017). Similar to the RNA-seq analysis, very few TF consensus sequences were enriched in the promoters of genes upregulated upon shPBRM1, but the main consensus sequences enriched were associated with MBTPS2 (Figure 2C), a protease that activates TFs involved in cholesterol synthesis and ER stress response (Rawson, 2013), and YY1, a structural protein involved in promoter-enhancer associations (Beagan et al., 2017).

To further define whether these putative TFs are directly regulated by PBRM1's chromatin remodeling function, we next turned to Assay for Transposase-Accessible Chromatin (ATAC)-seq to identify sites of PBRM1-dependent chromatin accessibility. As observed elsewhere (Gao et al., 2017), PBRM1 knockdown did not have dramatic effects on global chromatin accessibility. It did, however, result in a significant decrease in accessibility (at least 1.5-fold) at 5,245 sites and increased accessibility at 6,790 in NMuMG cells (Figures 2D and 2E) with similar genomic distributions (Figure 2F). Similar results were obtained using PBRM1 knockdown in HK-2 epithelial cells (Figures S2A and S2B). To identify TFs that are potentially dependent on PBRM1 for chromatin binding, we calculated the enrichment of TF consensus binding sequences at sites with differential accessibility upon PBRM1 knockdown (Figures 2G and S2C). Several TF consensus sequences were significantly enriched compared with background at sites of increased and decreased accessibility upon shPBRM1. Consensus sequences for KLF, AP-1, ETS, FOXO, and NF-κB TFs were highly enriched in regions with decreased accessibility upon shPBRM1, which correlates with the predicted regulators based on RNA-seq data (Figure 2C). In addition, there was a significant overlap between genes downregulated upon shPBRM1 and genes with an associated region of decreased accessibility (536 genes, $p = 4.5x10^{83}$) and these regions displayed enrichment for KLF, AP-1, ETS, and FOXO consensus sequences. Although we observed similar enrichment of consensus sequence-binding sites in the regions with increased accessibility upon shPBRM1, the regions of accessibility did not correlate with genes upregulated upon shPBRM1 (144 genes, $p = 0.455$). As many of the biological pathways identified were related to apoptosis and stress response, we investigated the cooperation between PBRM1 and c-Jun and NRF2, two TFs that are activated during stress (Jiang et al., 2016; Rössler and Thiel, 2017) (Figure 2H). Using lentiviral-mediated shRNA knockdown, we found that similar to the PBRM1 knockout, knockdown of c-Jun (but not NRF2) increased proliferation (S2D). Using a publicly available dataset of NRF2 bound and regulated genes in A549 lung cancer cell lines (GSE113497), we identified 36 NRF2 targets that are also differentially expressed in the PBRM1 knockdown and have associated sites of decreased chromatin accessibility in the shPBRM1 ATAC-seq. Intriguingly, these included canonical NRF2 target antioxidant genes *HMOX1* and *NQO1* (Chorley et al., 2012). Using qRT-PCR we confirmed *NRF2* knockdown and evaluated the requirement for PBRM1 on expression of these genes (Figure 2H, left). In contrast to many published reports, *HMOX1* did not show a dependence on NRF2 for expression, although it was dependent on PBRM1. As expected, *NQO1* was dependent on both NRF2 and PBRM1 for expression. In the absence of comprehensive c-Jun datasets, we selected several putative c-Jun targets from c-Jun N-terminal kinase (JNK)-dependent genes identified in previous studies. These include *BCL2L1*, an anti-apoptotic regulator (Girnius and Davis, 2017); *HK2*, a metabolic enzyme and anti-apoptotic regulator (Insua-Rodríguez et al., 2018); and *IL1RL1*, an anti-inflammatory interleukin (IL)-33 receptor (Kim et al., 2015). We confirmed c-Jun knockdown in NMuMG cells using qRT-PCR and validated that these genes are regulated by both PBRM1 and c-Jun (Figure 2H, right). In summary, genes affected by PBRM1 knockdown are targets of TFs involved in response to stress.

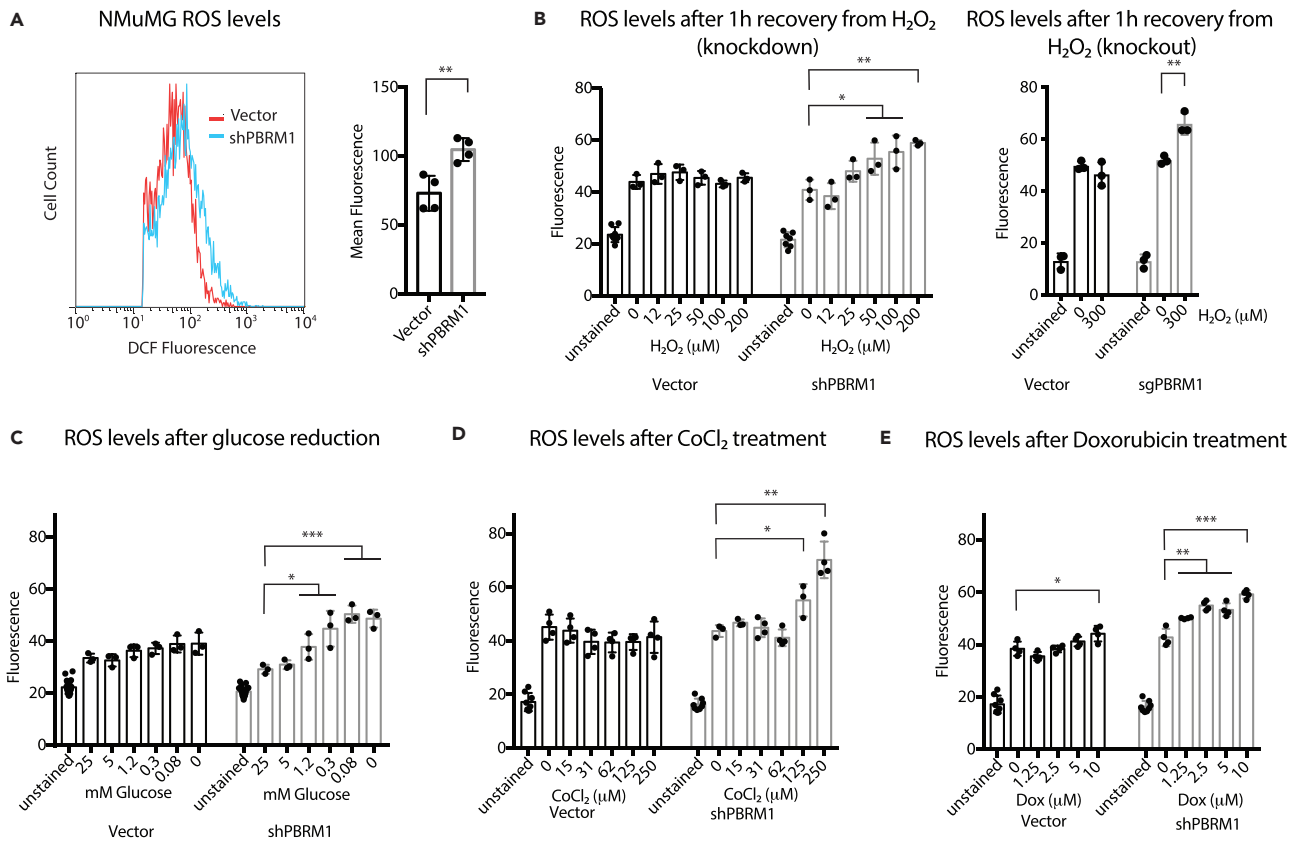

Figure 3. Knockdown of PBRM1 Results in Elevated ROS under Cellular Stress Conditions

(A) NMuMG cells were trypsinized and stained for 30 min with H_2-DCFDA, washed with PBS, and analyzed using flow cytometry. The mean fluorescence value for 10,000 cells was calculated from four independent experiments.

(B) NMuMG cells grown in 96-well plates were treated with increasing concentrations of H_2O_2 for 1 h, washed with PBS, and incubated with H_2-DCFDA for 30 min. Reagent was washed away, and the DCF fluorescence was measured in live cells.

(C) NMuMG cells grown in 96-well plates were treated with media containing varying concentrations of glucose (normal media = 25 mM) for 16 h, washed with PBS, and incubated with H_2-DCFDA for 30 min. Reagent was washed away, and the DCF fluorescence was measured in live cells.

(D) NMuMG cells grown in 96-well plates were treated with media containing varying concentrations of $CoCl_2$ for 24 h, washed with PBS, and incubated with H_2-DCFDA for 30 min. Reagent was washed away, and the DCF fluorescence was measured in live cells.

(E) NMuMG cells grown in 96-well plates were treated with media containing varying concentrations of doxorubicin for 24 h, washed with PBS, and incubated with H_2-DCFDA for 30 min. Reagent was washed away, and the DCF fluorescence was measured in live cells.

*p < 0.05, **p < 0.01, ***p < 0.001 (paired Student's t test). ns, not significant. Error bars represent S.D.

Knockdown of PBRM1 Results in Elevated ROS under Cellular Stress Conditions

Owing to the transcriptional signature indicating an increased importance for PBRM1 in regulating genes involved in stress response, we next examined how depletion of PBRM1 affects ROS, which are generated by cells under a variety of cellular stresses (Geou-Yarh Liou, 2010). NMuMG cells have low endogenous ROS levels, and PBRM1 knockdown results in a small but significant increase in ROS under normal cell culture conditions (Figure 3A), as measured by conversion of 2′,7′-dichlorodihydrofluorescein diacetate (H_2DCFDA) to the highly fluorescent 2′,7′-dichlorofluorescein (DCF) by intracellular ROS. To understand the effects of PBRM1 on ROS under high cellular stress, we looked at ROS levels after recovery from hydrogen peroxide treatment (Figure 3B), glucose deprivation (Figure 3C), hypoxia-inducing $CoCl_2$ treatment (Figure 3D), and DNA-damaging doxorubicin treatment (Figure 3E). Under all these stress conditions, cells lacking PBRM1 expression displayed increased levels of ROS.

PBRM1 Expression Is Cytoprotective under High-Stress Conditions

A low-level increase in ROS production promotes cancer progression by stimulating signaling, and facilitating transformation through increasing genomic instability and inflammation (Figure 4A) (Geou-Yarh

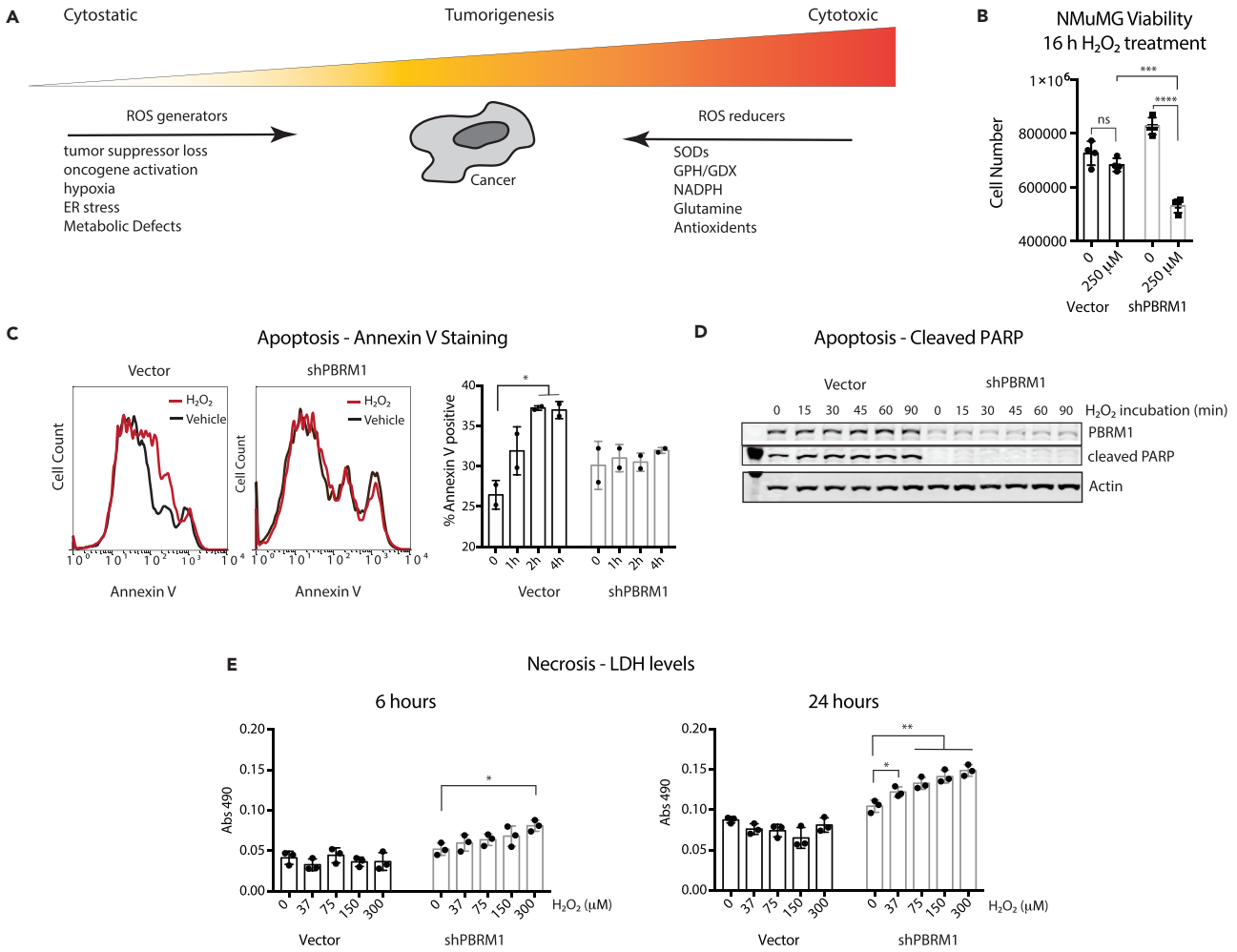

Figure 4. PBRM1 Expression Is Cytoprotective under High-Stress Conditions

PBRM1 induces apoptotic pathways and increases cellular viability under high-cellular-stress conditions.

(A) Depiction of the multifaceted role ROS regulators play in cancer.

(B) NMuMG cells were cultured in normal cell media or 250 μM H_2O_2 for 16 h, and the number of live cells were counted using trypan blue.

(C) Annexin V staining was measured in NMuMG cells treated with 200 μM H_2O_2 for the indicated times. The percentage of annexin V-positive cells was calculated for two independent experiments.

(D) Whole-cell lysates were prepared from NMuMG cells treated with 200 μM H_2O_2 for the indicated times and probed for the indicated proteins using immunoblot analysis.

(E) LDH release was measured from 10 μL media using LDH Cytotoxicity Assay Kit II (Abcam).

*p < 0.05, **p < 0.01, ***p < 0.001, ****p < 0.0001 (paired Student's t test). ns, not significant. Error bars represent SD. Also see Figure S3.

Liou, 2010). In addition, ROS can increase AKT phosphorylation and induce changes in cell adhesion molecules to increase motility (Geou-Yarh Liou, 2010), both of which we observed previously in Caki2 renal cancer cells without PBRM1 (Chowdhury et al., 2016) and in epithelial cells lacking PBRM1 (Figure S1A). Although increases in ROS are characteristic in cancer and contribute to transformation and oncogenesis, cancer cells need to avoid extremely high levels of ROS due to cytotoxicity (Figure 4A) (Geou-Yarh Liou, 2010). To understand how PBRM1-regulated ROS levels under high-stress conditions affect cellular viability, we measured cell survival after high concentrations of hydrogen peroxide for 16 h. We found that PBRM1 knockdown decreased viability under these high-stress conditions in the NMuMG (Figure 4B) and MDCK epithelial cells (Figure S3A), an effect observed similarly with the NRF2 knockdown (Figure S3B). This was not due to increased apoptosis in the PBRM1 knockdown, and in fact, cells lacking PBRM1 displayed a deficiency in annexin V (Figure 4C) and cleaved PARP (Figures 4D and S3C) under stress conditions. This is in line with the transcriptional role for PBRM1 in regulating pro-apoptotic genes (Figure 2A).

Although it seems counterintuitive that PBRM1-expressing cells have both increased apoptosis and increased cell survival under high-stress conditions, it is consistent with a role for PBRM1 in the stress response, which often results in apoptosis if cellular stresses are not resolved. In contrast, cells lacking PBRM1 are unable to mount a proper response to external stress, leading to high ROS levels and cell death through other means, such as necrosis (Fulda et al., 2010), which is supported by the increase in necrosis marker lactate dehydrogenase (LDH) in the NMuMG cells lacking PBRM1 (Figure 4E).

PBRM1-Regulated Transcriptional Effects under Cellular Stress Conditions

To determine if the dependency on PBRM1 expression for viability under stress conditions is due to PBRM1's regulation of different genes under stress conditions, we characterized the transcriptional profile of NMuMG cells with and without PBRM1 knockdown, grown in H_2O_2 (200 μM) for 2 h or low-glucose media for 6 h. There were between 1,000 and 2,000 differentially expressed genes (DEGs) identified in cells grown in H_2O_2 or low-glucose growth conditions for both vector control and shPBRM1 cells (Table S1); however, the impact of PBRM1 knockdown on overall gene expression was more significant than the impact of either stress conditions (Figure 5A). We observed a significant correlation between gene expression changes induced by PBRM1 knockdown in different stress conditions (Figure S4A), and a significant correlation between gene expression changes induced by stress conditions in the two cell lines (vector and shPBRM1) (Figure S4B) indicating that many genes altered by stress are not dependent on PBRM1 and many genes dependent on PBRM1 are not altered by stress (Figure S4C). In addition, we observed a significant correlation between gene expression changes induced by the two different stress conditions (Figure S4C). As expected, the significantly enriched GO terms were similar for genes regulated by PBRM1 under stress treatment compared with untreated cells; however, more genes from pathways involved in cell adhesion, signaling, and apoptosis were altered upon shPBRM1 under stress treatments (Figure 5B). Furthermore, we observed several GO terms that were significantly enriched only for genes downregulated with shPBRM1 under either stress treatment, including cell cycle, protein metabolic processes, and cellular response to stress, and for genes downregulated upon shPBRM1 only under H_2O_2 treatment, such as RNA processing and DNA damage response (Figure 5C). Accordingly, there were many genes dependent on PBRM1 expression for induction under H_2O_2 stress (Figure 5D), many of which are involved in cell adhesion, apoptosis, ER stress, and antioxidant response. We used this dataset to identify the NRF2 and c-Jun targets from Figure 2 that were induced under H_2O_2 stress. c-Jun target, *IL1RL1*, an IL-33 receptor involved in protection from stress (Kim et al., 2015), requires both PBRM1 and c-Jun for induction upon H_2O_2 treatment (Figure 5E). Similarly, the antioxidant NRF2 targets, *HMOX1* and *NQO1*, are induced upon H_2O_2 treatment and require PBRM1 and/or NRF2 for full gene induction (Figure 5F). In conclusion, the RNA-seq analysis of PBRM1-dependent gene expression under stress conditions supports a role for PBRM1 in inducing a subset of stress response genes to promote cell survival under conditions of high stress.

PBRM1 Has Cell-Type-Specific Roles in Viability

After establishing that PBRM1 knockdown can have different effects on viability depending on the stress environment, we re-evaluated the premature senescence phenotype previously described for PBRM1 knockout in mouse embryonic fibroblasts (MEFs) (Lee et al., 2016). We confirmed that PBRM1 knockdown (Figure S5A) results in a loss in the proliferative capacity of MEFs (Figure 6A) similar to published findings with the PBRM1 conditional knockout (Lee et al., 2016). We next observed a significant increase in ROS levels and H_2O_2 levels in MEFs upon PBRM1 knockdown (Figure 6B and S5B), which was most similar to the robust increase in ROS levels observed in shPBRM1 NMuMG cells grown under high-stress conditions. This particular sensitivity of MEFs to PBRM1 knockdown is most likely due to the unique susceptibility of MEFs to oxidative stress from high oxygen content in air (Espana-Agusti et al., 2017). To support this, we found that exogenous antioxidants such as vitamin C (Figure 6C) or *N*-acetylcysteine (Figure S5C) were able to reverse the viability defect induced by PBRM1 knockdown in MEFs.

We next sought to examine how intrinsic genetic changes could alter dependency on PBRM1. To do this we employed the MCF10A human mammary epithelial cell line (Soule et al., 1990), and the MCF10A-T1k cell line, which has been transformed with T24-HRas and passaged in a mouse (Dawson et al., 1996). We knocked down PBRM1 in both these cell lines (Figure S6A) and found dramatically different effects on viability. Similar to other epithelial cell lines, PBRM1 knockdown in MCF10A results in an increase in proliferation and a slight increase in ROS (Figure 6D), with some, but not all, of the same changes in gene expression compared with PBRM1 knockdown in NMuMG cells (Figure S6B), In contrast, PBRM1 knockdown in the MCF10A-T1k cell line is highly deleterious to viability, causing cells to cease proliferation altogether within

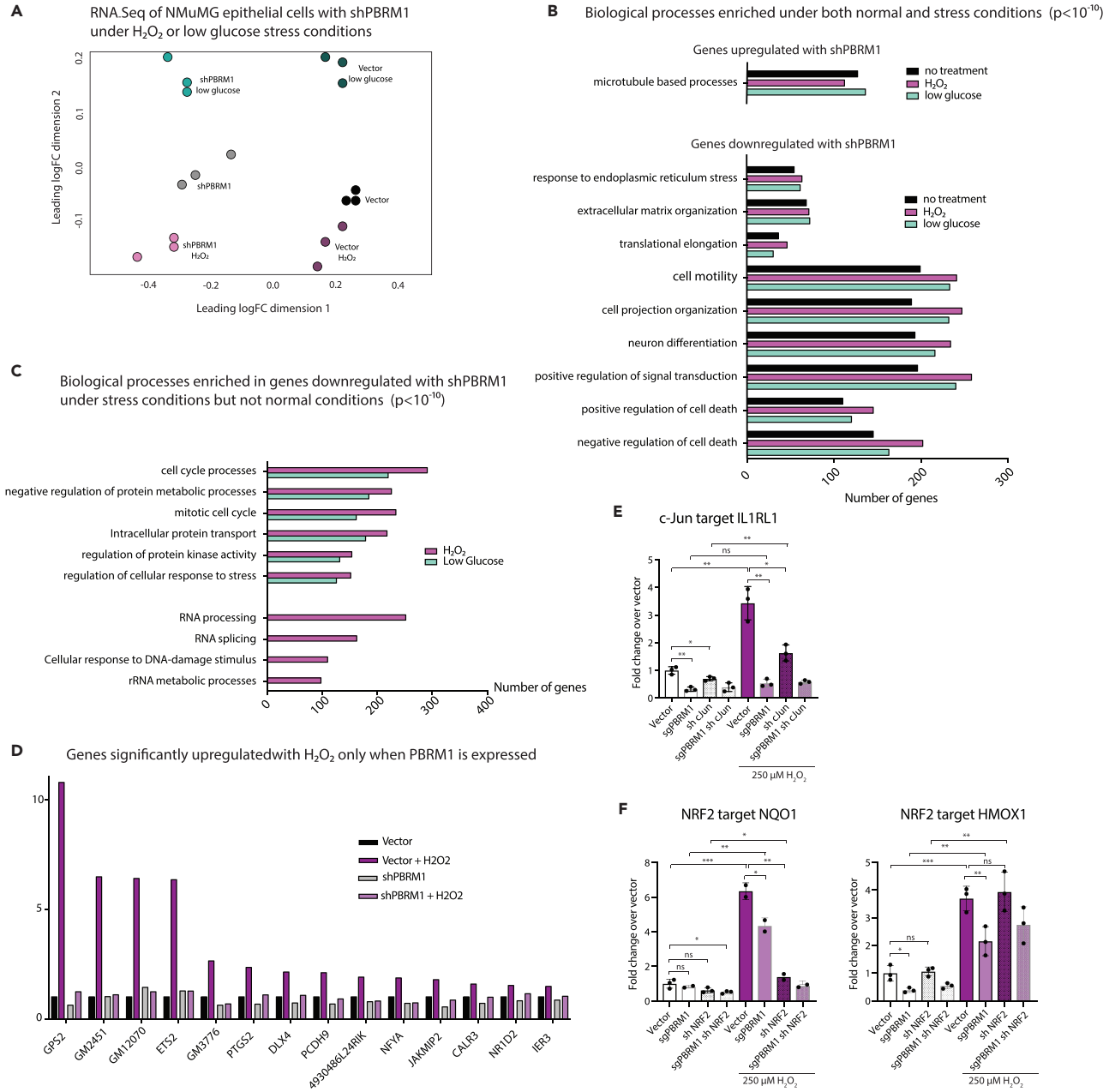

Figure 5. PBRM1-Regulated Transcriptional Effects under Cellular Stress Conditions

(A) RNA-seq was performed on NMuMG cells grown in 200 μM H_2O_2 for 2 h or glucose-free media for 6 h.

(B) Top overrepresented biological process GO terms ($p < 10^{-10}$) for genes differentially expressed upon shPBRM1 in all cell culture conditions.

(C) Overrepresented biological process GO terms ($p < 10^{-10}$) for differentially expressed genes downregulated with shPBRM1 only under H_2O_2 or low-glucose cell culture conditions.

(D) Representation of the RNA-seq data for a subset of differentially expressed genes that require PBRM1 for upregulation during H_2O_2 stress.

(E) The contribution of PBRM1 to the transcriptional regulation of c-Jun target gene *IL1RL1* under normal cell culture or 4 h H_2O_2 (250 μM) using qRT-PCR and *OAZ1* as the housekeeping gene. n = 3.

(F) The contribution of PBRM1 to the transcriptional regulation of NRF2 target genes *NQO1* (left) and *HMOX1* (right) under normal cell culture or 4 h H_2O_2 (250 μM) using qRT-PCR and *OAZ1* as the housekeeping gene. n = 3.

*p < 0.05, **p < 0.01, ***p < 0.001 (paired Student's t test). ns, not significant. Error bars represent SD. Also see Figure S4 and Table S1.

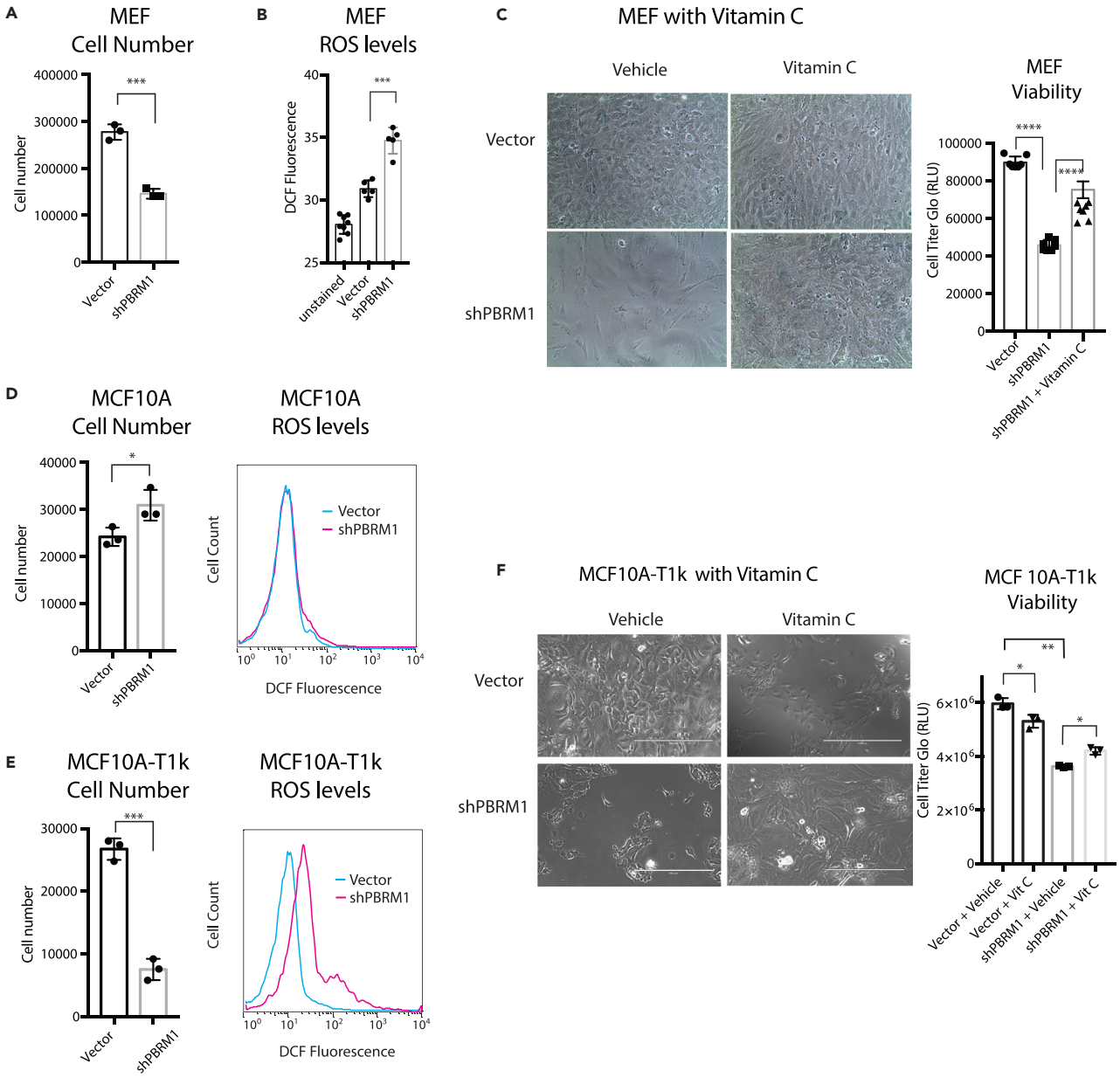

Figure 6. PBRM1 has Cell-Type-Specific Roles on Viability

(A) Mouse embryonic fibroblasts (MEFs) were counted after 72 h growth using trypan blue and data presented as mean ± SD. n = 3.

(B) Equal numbers of MEFs were plated in 96-well format. After 24 h the cells were washed with PBS, incubated with H2-DCFDA for 1 h, and the DCF fluorescence was measured in live cells. Data are presented as mean ± SD. n = 5.

(C) MEFs were cultured for 8 days in normal media or media supplemented with 20 μg/mL vitamin C. Luminescence was measured using CellTiter-Glo assay system and data presented as mean ± SD. n = 7.

(D) Human mammary epithelial cell line MCF10A was counted after 72 h growth using trypan blue to eliminate dead cells (left), and data are presented as mean ± SD. n = 3. MCF10A cells were trypsinized and stained for 30 min with H_2-DCFDA, washed with PBS, and 100,000 cells were analyzed using flow cytometry (right).

(E) Transformed human mammary cell line MCF10A-T1k was counted after 72 h growth using trypan blue to eliminate dead cells (left), and data are presented as mean ± SD. n = 3. MCF10A-T1k cells were trypsinized and stained for 30 min with H_2-DCFDA, washed with PBS, and 100,000 cells were analyzed using flow cytometry (right).

(F) MCF10A-T1k cells were cultured for 7 days in normal media or media supplemented with 20 μg vitamin C (left). Luminescence was measured using CellTiter-Glo assay system (right) and data presented as mean ± SD. n = 3.

*p < 0.05, **p < 0.01, ***p < 0.001, ****p < 0.0001 (paired Student's t test). ns, not significant. Error bars represent SD. Also see Figures S5 and S6.

three to four passages (Figure 6E, left). Similar to MEFs, PBRM1 knockdown in this line induces a highly significant increase in ROS levels (Figure 6E, right), and similar to MEFs, vitamin C administration can partially restore proliferative capacity in the PBRM1 knockdown (Figure 6F). The oncogene-induced stress in the MCF10A-T1k cell line promotes dependency on PBRM1 for viability, which may be reflected in its increased level of ROS at baseline compared with MCF10A cells (Figure S6C). In summary, our data up to this point establish that PBRM1 knockdown can have different effects on viability in the same cell line due to different external stress environments, or in two different cell lines due to cell type susceptibilities to stress.

PBRM1 Displays Stress Response Phenotype in Renal Cancer Cells

To begin to decipher how the stress response functions observed for PBRM1 in epithelial cells might relate to its role in renal carcinoma, we first determined the enriched GO terms for the genes with decreased expression in patients with PBRM1 mutations, which were similar to the pathways observed in the NMuMG cells, including cell adhesion, neuronal processes, apoptosis, and ER stress or proteolysis (Figure S7A). Furthermore, we compared the differentially regulated genes and observed the most significant gene overlap between genes with decreased expression in patients with PBRM1 mutations and genes with decreased expression in the PBRM1 knockdown (S7B), similar to the overlaps we observed with Caki2 cells, a renal carcinoma cell line with loss-of-function mutations in PBRM1 (Chowdhury et al., 2016). Therefore we used Caki2 ccRCC cell lines with PBRM1 re-expression to determine if the same phenotypes are observed in the renal cancer setting. Previously we have shown that re-expression of PBRM1 decreases growth and migration of Caki2 cells (Chowdhury et al., 2016). When we used DCF staining to determine ROS levels, we observed highly elevated ROS compared with the epithelial cells, which is consistent with previous observations about high ROS in cancer cell lines (Geou-Yarh Liou, 2010) (Figures 3A and 7A). However, the re-expression of PBRM1 only reduced ROS levels to a very slight degree under normal cell culture conditions (Figure 7A). In contrast to the NMuMG cells, high-stress conditions in Caki2 cells did not result in an increase in ROS levels in the absence of PBRM1; however, in the presence of PBRM1, high-stress conditions induced a dramatic decrease in ROS levels (Figures 7B and 7C). Furthermore, PBRM1 re-expression promoted cell survival under high-stress conditions (Figure 7D), similar to the phenotype observed in NMuMG cells (Figure 4B). Also similar to the phenotype observed in NMuMG cells, Caki2 cells with PBRM1 re-expression display a greater increase in cleaved PARP, an apoptosis marker, under hydrogen peroxide treatment conditions (Figure 7E). Activation of apoptosis seems conflicting with PBRM1's role in survival, whereas it is consistent with a role for PBRM1 in activating stress response pathways that eventually lead to apoptosis under continued cellular stress (Fulda et al., 2010). In contrast, Caki2 cells lacking PBRM1 display an increase in LDH when exposed to H_2O_2 stress, indicative of eventual necrosis from failing to properly activate stress response pathways (Figure 7F).

DISCUSSION

Chromatin regulators are frequently misregulated in cancer with resulting alterations in gene transcription; however, many of these regulators alter a large number of genes to a small degree and can regulate very different sets of genes in different cell lines. An additional challenge resides in the fact that many chromatin regulators modulate transcription differently depending on environmental inputs (Johnson and Dent, 2013). Thus it has been incredibly challenging to decipher how the transcriptional effects of chromatin regulators observed in a particular cell line relate to its general biochemical function or its phenotype *in vivo*. Traditional cell culture models are often devoid of the environmental stimuli chromatin regulators normally sense, making it a significant challenge to develop a relevant cell culture model for accurately studying these regulators. Here, we have used transcriptional analysis of epithelial cells with PBRM1 knockdown to identify pathways involved in epithelial cell maintenance and stress response. In addition, we have validated a role for PBRM1 in the maintenance of epithelial cell identity and identified KLF, AP-1, and ETS TFs consensus sequences in both genes downregulated upon shPBRM1 and regions with decreased chromatin accessibility upon shPBRM1. From this, we have validated a role for PBRM1 in facilitating the transcription of c-Jun and NRF2 target genes, restraining ROS production and inducing both apoptotic and cell survival pathways under high-stress conditions (Roupé et al., 2014; Wang et al., 2014).

In addition to changes in TF expression and localization during cellular stress, oxidative stress and metabolic stress are known to specifically upregulate H3K14Ac at stress response genes (Schram et al., 2013), a histone mark specifically recognized by PBRM1 (Porter and Dykhuizen, 2017). H3K14Ac is generally found at active promoters with H3K9Ac, whereas it is found without H3K9Ac at inducible genes (Karmodiya et al., 2012) and is specifically increased in gene bodies during stress (Johnsson et al., 2009). H3K14Ac is also a

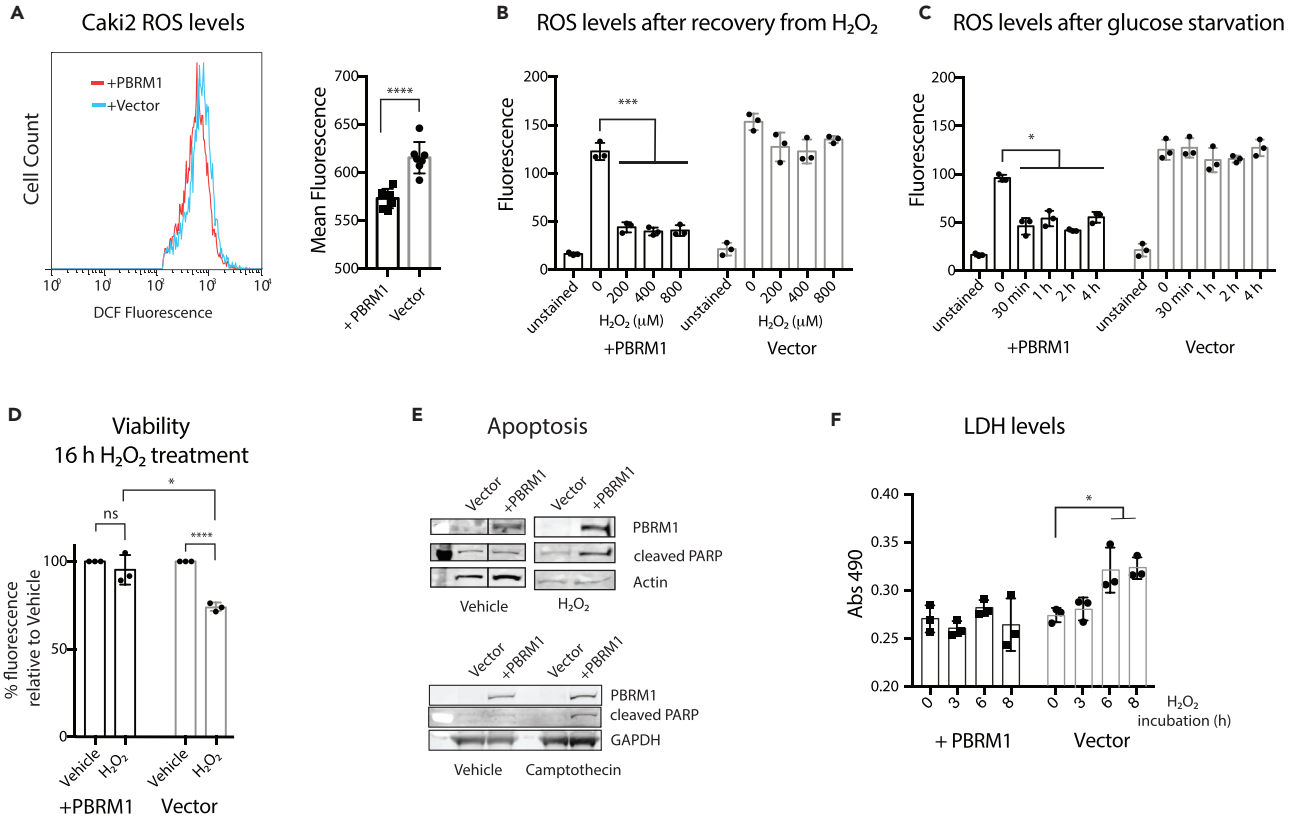

Figure 7. PBRM1 Displays Stress Response Phenotype in Renal Cancer Cells

PBRM1 regulates stress response in renal carcinoma cells.

(A) Caki2 cells were trypsinized and stained for 30 min with H_2-DCFDA, washed with PBS, and analyzed using flow cytometry. The mean fluorescence value for 10,000 cells was calculated from seven independent experiments.

(B) Caki2 cells grown in 96-well plates were treated with increasing concentrations of H_2O_2 for 1 h, washed with PBS, and incubated with H_2-DCFDA for 30 min. Reagent was washed away, and the DCF fluorescence was measured in live cells.

(C) Caki2 cells grown in 96-well plates were treated with glucose-free media for varying time periods, washed with PBS, and incubated with H_2-DCFDA for 30 min. Reagent was washed away, and the DCF fluorescence was measured in live cells.

(D) Caki2 cells were cultured in normal cell media or 200 μM H_2O_2 for 16 h, and the cell viability was estimated using crystal violet staining.

(E) Whole-cell lysates were prepared from Caki2 cells treated with 200 μM H_2O_2 or 100 μM camptothecin for 2 h, and relative levels of indicated proteins were probed using immunoblot analysis. Irrelevant lane was spliced out.

(F) LDH release was measured from 10 μL media using LDH Cytotoxicity Assay Kit II (Abcam).

*p < 0.05, ***p < 0.001, ****p < 0.0001 (paired Student's t test). ns, not significant. Error bars represent SD. Also see Figure S7.

mark associated with renal epithelium adaptation to oxidative stress (Mahalingaiah et al., 2016, 2015), high-fat-diet-induced inflammation in rodents (Suter et al., 2012), ER stress (Dicks et al., 2015), and sites of DNA damage (Chiu et al., 2017), a process for which PBRM1 has a well-established role (Kakarougkas et al., 2014). Therefore specific patterns of histone acetylation likely delineate a subset of stress response genes targeted by PBRM1, which is likely to be unique for a particular cell type, as well as a particular stressor.

A role for PBRM1 in stress response is in agreement with recent findings that PBRM1 deletion alone is not sufficient for transformation but acts to facilitate oncogenesis in cooperation with VHL deletion (Espana-Agusti et al., 2017; Gu et al., 2017; Nargund et al., 2017). PBRM1 deletion allows for an amplification of oncogenic signaling (Gao et al., 2017; Nargund et al., 2017), as well as a bypass of checkpoints induced by replication stress after VHL deletion (Espana-Agusti et al., 2017). This could be in part due to PBRM1's role in regulating the hypoxic stress response in cooperation with HIF1a, which allows for the reduction of ROS and induction of apoptosis in response to hypoxia (Kim et al., 2006).

A role in stress response is likely part of PBRM1's function as a tumor suppressor during cancer initiation, and it may also be involved in PBRM1's protective function against cancer therapeutics, similar to the

protective role PBRM1 plays under high-stress conditions. Patients with ccRCC with PBRM1 mutations tend to have favorable prognosis (Piva et al., 2015), and recent studies indicate that PBRM1 mutant tumors respond particularly well to sunitinib (Beuselinck et al., 2017) and PD-1 inhibitors (Miao et al., 2018). In support of this, a recent CRISPR-Cas9 screen identified PBRM1, along with other PBAF-specific subunits, as resistance factors against T cell-mediated killing (Pan et al., 2018). This is related to a general role for PBRM1 in suppressing the inflammatory response, as PBRM1 deletion also increases innate immunity hyperinflammation in the gut (He et al., 2017; Shu et al., 2017). The general role for PBRM1 in stress response could relate to PBRM1's role in suppressing inflammation (and T cell-mediated toxicity) through the regulation of homeostasis (Chovatiya and Medzhitov, 2014), although that connection will need to be explored further.

Limitations of Study

Using epithelial cell lines, we have defined a role for PBRM1 in mediating the expression of stress response genes. Although this finding unifies the disparate results previously published regarding PBRM1's cellular function and provides a framework for future studies, it does not provide a precise mechanism for PBRM1's function. In addition, although we observe similar functions for PBRM1 in a renal cancer cell line, our work does not make any conclusions about whether PBRM1's role in the transcription of stress response genes is its primary function as a tumor suppressor during renal carcinoma progression. Lastly, although a transcriptional role in stress response is typical for chromatin regulators involved in DNA damage repair (Gregersen and Svejstrup, 2018), we have not defined here whether the observed role for PBRM1 in upregulating stress response genes is truly independent from its role in DNA damage repair. Additional mechanistic work will be required to dissect these functions on a molecular level.

METHODS

All methods can be found in the accompanying Transparent Methods supplemental file.

DATA AND SOFTWARE AVAILABILITY

Data sets generated in these experiments are available at the Gene Expression Omnibus under accession number GSE113606.

SUPPLEMENTAL INFORMATION

Supplemental Information can be found online at https://doi.org/10.1016/j.isci.2019.04.027.

ACKNOWLEDGMENTS

This research was supported by grants from the NIH (U01CA207532 to E.C.D., R01CA207751 to M.W.K., K22HL125593 to M.K.). This work was supported by the Office of the Assistant Secretary of Defense for Health Affairs, through the Peer Reviewed Cancer Research Program, under Award No. W81XWH-17-1-0267 to ECD. Opinions, interpretations, conclusions, and recommendations are those of the author and are not necessarily endorsed by the Department of Defense. E.C.D. was supported by The V Foundation for Cancer Research (V2014-004 and D2016-030). E.G.P. was supported by the Borch Graduate Fellowship from the Purdue Department of Medicinal Chemistry and Molecular Pharmacology. Additional support was from the Purdue University Center for Cancer Research, NIH grant P30 CA023168 for shared resources and the Small Grants Program..

AUTHOR CONTRIBUTIONS

E.G.P., A.D., B.C., and E.C.D. conceived the experiments. E.G.P., A.D., B.C., M.K.W., and E.C.D. designed the experiments. E.G.P., A.D., B.C., J.C.S., and H.L. performed experiments. B.C. and B.C.C. performed bioinformatics analyses. M.K. provided advice for ATAC-seq analysis. E.G.P., A.D., and E.C.D. wrote the manuscript with assistance from B.C. and B.C.C.

DECLARATION OF INTERESTS

The authors declare no competing interests.

Received: September 6, 2018
Revised: March 10, 2019
Accepted: April 19, 2019
Published: May 31, 2019

REFERENCES

Beagan, J.A., Duong, M.T., Titus, K.R., Zhou, L., Cao, Z., Ma, J., Lachanski, C.V., Gillis, D.R., and Phillips-Cremins, J.E. (2017). YY1 and CTCF orchestrate a 3D chromatin looping switch during early neural lineage commitment. Genome Res. *27*, 1139–1152.

Berglund, F.M., Weerasinghe, N.R., Davidson, L., Lim, J.C., Eickholt, B.J., and Leslie, N.R. (2012). Disruption of epithelial architecture caused by loss of PTEN or by oncogenic mutant p110α/PIK3CA but not by HER2 or mutant AKT1. Oncogene *32*, 4417–4426.

Beuselinck, B., Verbiest, A., Couchy, G., Job, S., de Reynies, A., Meiller, C., Albersen, M., Verkarre, V., Lerut, E., Méjean, A., et al. (2017). Pro-angiogenic gene expression is associated with better outcome on sunitinib in metastatic clear-cell renal cell carcinoma. Acta Oncol. *57*, 498–508.

Brownlee, P.M., Chambers, A.L., Cloney, R., Bianchi, A., and Downs, J.A. (2014). BAF180 promotes cohesion and prevents genome instability and aneuploidy. Cell Rep. *6*, 973–981.

Cancer Genome Atlas Research Network (2013). Comprehensive molecular characterization of clear cell renal cell carcinoma. Nature *499*, 43–49.

Charlop-Powers, Z., Zeng, L., Zhang, Q., and Zhou, M.-M. (2010). Structural insights into selective histone H3 recognition by the human Polybromo bromodomain 2. Cell Res. *20*, 529–538.

Chiu, L.-Y., Gong, F., and Miller, K.M. (2017). Bromodomain proteins: repairing DNA damage within chromatin. Philos. Trans. R. Soc. Lond. B Biol. Sci. *372*, 20160286.

Chorley, B.N., Campbell, M.R., Wang, X., Karaca, M., Sambandan, D., Bangura, F., Xue, P., Pi, J., Kleeberger, S.R., and Bell, D.A. (2012). Identification of novel NRF2-regulated genes by ChIP-Seq: influence on retinoid X receptor alpha. Nucleic Acids Res. *40*, 7416–7429.

Chovatiya, R., and Medzhitov, R. (2014). Stress, inflammation, and Defense of homeostasis. Mol. Cell *54*, 281–288.

Chowdhury, B., Porter, E.G., Stewart, J.C., Ferreira, C.R., Schipma, M.J., and Dykhuizen, E.C. (2016). PBRM1 regulates the expression of genes involved in metabolism and cell adhesion in renal clear cell carcinoma. PLoS One *11*, e0153718.

Cohet, N., Stewart, K.M., Mudhasani, R., Asirvatham, A.J., Mallappa, C., Imbalzano, K.M., Weaver, V.M., Imbalzano, A.N., and Nickerson, J.A. (2010). SWI/SNF chromatin remodeling enzyme ATPases promote cell proliferation in normal mammary epithelial cells. J. Cell. Physiol. *223*, 667–678.

Dawson, P.J., Wolman, S.R., Tait, L., Heppner, G.H., and Miller, F.R. (1996). MCF10AT: a model for the evolution of cancer from proliferative breast disease. Am. J. Pathol. *148*, 313–319.

Dicks, N., Gutierrez, K., Michalak, M., Bordignon, V., and Agellon, L.B. (2015). Endoplasmic reticulum stress, genome damage, and cancer. Front. Oncol. *5*, 61.

Duan, M.R., and Smerdon, M.J. (2014). Histone H3 lysine 14 (H3K14) acetylation facilitates DNA repair in a positioned nucleosome by stabilizing the binding of the chromatin remodeler RSC (remodels structure of chromatin). J. Biol. Chem. *289*, 8353–8363.

Espana-Agusti, J., Warren, A., Chew, S.K., Adams, D.J., and Matakidou, A. (2017). Loss of PBRM1 rescues VHL dependent replication stress to promote renal carcinogenesis. Nat. Commun. *8*, 2026.

Fulda, S., Gorman, A.M., Hori, O., and Samali, A. (2010). Cellular stress responses: cell survival and cell death. Int. J. Cell Biol. *2010*, 1–23.

Gao, W., Li, W., Xiao, T., Liu, X.S., and Kaelin, W.G. (2017). Inactivation of the PBRM1 tumor suppressor gene amplifies the HIF-response in VHL / clear cell renal carcinoma. Proc. Natl. Acad. Sci. U S A *114*, 1027–1032.

Geou-Yarh Liou, P.S. (2010). Reactive oxygen species in cancer. Free Radic. Res. *44*, 479–496.

Gerlinger, M., Horswell, S., Larkin, J., Rowan, A.J., Salm, M.P., Varela, I., Fisher, R., McGranahan, N., Matthews, N., Santos, C.R., et al. (2014). Genomic architecture and evolution of clear cell renal cell carcinomas defined by multiregion sequencing. Nat. Genet. *46*, 225–233.

Ghaleb, A.M., McConnell, B.B., Kaestner, K.H., and Yang, V.W. (2011). Altered intestinal epithelial homeostasis in mice with intestine-specific deletion of the Krüppel-like factor 4 gene. Dev. Biol. *349*, 310–320.

Girnius, N., and Davis, R.J. (2017). JNK promotes epithelial cell anoikis by transcriptional and post-translational regulation of BH3-only proteins. Cell Rep. *21*, 1910–1921.

Gregersen, L.H., and Svejstrup, J.Q. (2018). The cellular response to transcription-blocking DNA damage. Trends Biochem. Sci. *43*, 327–341.

Gu, Y.-F., Cohn, S., Christie, A., McKenzie, T., Wolff, N.C., Do, Q.N., Madhuranthakam, A., Pedrosa, I., Wang, T., Dey, A., et al. (2017). Modeling renal cell carcinoma in mice: Bap1 and Pbrm1 inactivation drive tumor grade. Cancer Discov. *7*, 900–917.

Hall, H.G., Farson, D.A., and Bissell, M.J. (1982). Lumen formation by epithelial cell lines in response to collagen overlay: a morphogenetic model in culture. Proc Natl. Acad. Sci. U S A *79*, 4672–4676.

He, X., Yu, J., Wang, M., Cheng, Y., Han, Y., Yang, S., Shi, G., Sun, L., Fang, Y., Gong, S.-T., et al. (2017). Bap180/Baf180 is required to maintain homeostasis of intestinal innate immune response in *Drosophila* and mice. Nat. Microbiol. *2*, 17056.

Huang, X., Gao, X., Diaz-Trelles, R., Ruiz-Lozano, P., and Wang, Z. (2008). Coronary development is regulated by ATP-dependent SWI/SNF chromatin remodeling component BAF180. Dev. Biol. *319*, 258–266.

Huang, L., Peng, Y., Zhong, G., Xie, W., Dong, W., Wang, B., Chen, X., Gu, P., He, W., Wu, S., et al. (2015). PBRM1 suppresses bladder cancer by cyclin B1 induced cell cycle arrest. Oncotarget *6*, 16366–16378.

Insua-Rodríguez, J., Pein, M., Hongu, T., Meier, J., Descot, A., Lowy, C.M., De Braekeleer, E., Sinn, H.-P., Spaich, S., Sütterlin, M., et al. (2018). Stress signaling in breast cancer cells induces matrix components that promote chemoresistant metastasis. EMBO Mol. Med. *10*, e9003.

Jiang, S., Zhang, E., Zhang, R., and Li, X. (2016). Altered activity patterns of transcription factors induced by endoplasmic reticulum stress. BMC Biochem. *17*, 33.

Johnson, D.G., and Dent, S.Y.R. (2013). Chromatin: receiver and quarterback for cellular signals. Cell *152*, 685–689.

Johnsson, A., Durand-Dubief, M., Xue-Franzén, Y., Rönnerblad, M., Ekwall, K., and Wright, A. (2009). HAT-HDAC interplay modulates global histone H3K14 acetylation in gene-coding regions during stress. EMBO Rep. *10*, 1009–1014.

Kadoch, C., Hargreaves, D.C., Hodges, C., Elias, L., Ho, L., Ranish, J., and Crabtree, G.R. (2013). Proteomic and bioinformatic analysis of mammalian SWI/SNF complexes identifies extensive roles in human malignancy. Nat. Genet. *45*, 592–601.

Kaeser, M.D., Aslanian, A., Dong, M.-Q., Yates, J.R., and Emerson, B.M. (2008). BRD7, a novel PBAF-specific SWI/SNF subunit, is required for target gene activation and repression in embryonic stem cells. J. Biol. Chem. *283*, 32254–32263.

Kakarougkas, A., Ismail, A., Chambers, A.L., Riballo, E., Herbert, A.D., Künzel, J., Löbrich, M., Jeggo, P.A., and Downs, J.A. (2014). Requirement for PBAF in transcriptional repression and repair at DNA breaks in actively transcribed regions of chromatin. Mol. Cell *55*, 723–732.

Kalluri, R., and Weinberg, R.A. (2009). The basics of epithelial-mesenchymal transition. J. Clin. Invest. *119*, 1420–1428.

Karmodiya, K., Krebs, A.R., Oulad-Abdelghani, M., Kimura, H., and Tora, L. (2012). H3K9 and H3K14 acetylation co-occur at many gene

regulatory elements, while H3K14ac marks a subset of inactive inducible promoters in mouse embryonic stem cells. BMC Genomics *13*, 424.

Kim, J.-W., Tchernyshyov, I., Semenza, G.L., and Dang, C.V. (2006). HIF-1-mediated expression of pyruvate dehydrogenase kinase: a metabolic switch required for cellular adaptation to hypoxia. Cell Metab. *3*, 177–185.

Kim, J.Y., Lim, S.-C., Kim, G., Yun, H.J., Ahn, S.-G., and Choi, H.S. (2015). Interleukin-33/ST2 axis promotes epithelial cell transformation and breast tumorigenesis via upregulation of COT activity. Oncogene *34*, 4928–4938.

Lee, H.-S., Park, J.-H., Kim, S.-J., Kwon, S.-J., and Kwon, J. (2010). A cooperative activation loop among SWI/SNF, γ-H2AX and H3 acetylation for DNA double-strand break repair. EMBO J. *29*, 1434–1435.

Lee, H., Dai, F., Zhuang, L., Xiao, Z.-D., Kim, J., Zhang, Y., Ma, L., You, M.J., Wang, Z., and Gan, B. (2016). BAF180 regulates cellular senescence and hematopoietic stem cell homeostasis through p21. Oncotarget *7*, 19134–19146.

Mahalingaiah, P.K.S., Ponnusamy, L., and Singh, K.P. (2015). Chronic oxidative stress leads to malignant transformation along with acquisition of stem cell characteristics, and epithelial to mesenchymal transition in human renal epithelial cells. J. Cell. Physiol. *230*, 1916–1928.

Mahalingaiah, P.K.S., Ponnusamy, L., and Singh, K.P. (2016). Oxidative stress-induced epigenetic changes associated with malignant transformation of human kidney epithelial cells. Oncotarget *8*, 11127–11143.

Miao, D., Margolis, C.A., Gao, W., Voss, M.H., Li, W., Martini, D.J., Norton, C., Bossé, D., Wankowicz, S.M., Cullen, D., et al. (2018). Genomic correlates of response to immune checkpoint therapies in clear cell renal cell carcinoma. Science *359*, 801–806.

Mo, D., Li, C., Liang, J., Shi, Q., Su, N., Luo, S., Zeng, T., and Li, X. (2015). Low PBRM1 identifies tumor progression and poor prognosis in breast cancer. Int. J. Clin. Exp. Pathol. *8*, 9307–9313.

Murakami, A., Wang, L., Kalhorn, S., Schraml, P., Rathmell, W.K., Tan, A.C., Nemenoff, R., Stenmark, K., Jiang, B.-H., Reyland, M.E., et al. (2017). Context-dependent role for chromatin remodeling component PBRM1/BAF180 in clear cell renal cell carcinoma. Oncogenesis *6*, e287.

Nargund, A.M., Pham, C.G., Dong, Y., Wang, P.I., Osmangeyoglu, H.U., Xie, Y., Aras, O., Han, S., Oyama, T., Takeda, S., et al. (2017). The SWI/SNF protein PBRM1 restrains VHL-loss-driven clear cell renal cell carcinoma. Cell Rep. *18*, 2893–2906.

Pan, D., Kobayashi, A., Jiang, P., de Andrade, L.F., Tay, R.E., Luoma, A., Tsoucas, D., Qiu, X., Lim, K., Rao, P., et al. (2018). A major chromatin regulator determines resistance of tumor cells to T cell–mediated killing. Science *359*, 770–775.

Peña-Llopis, S., Vega-Rubín-de-Celis, S., Liao, A., Leng, N., Pavía-Jiménez, A., Wang, S., Yamasaki, T., Zhrebker, L., Sivanand, S., Spence, P., et al. (2012). BAP1 loss defines a new class of renal cell carcinoma. Nat. Genet. *44*, 751–759.

Piva, F., Santoni, M., Matrana, M.R., Satti, S., Giulietti, M., Occhipinti, G., Massari, F., Cheng, L., Lopez-Beltran, A., Scarpelli, M., et al. (2015). BAP1, PBRM1 and SETD2 in clear-cell renal cell carcinoma: molecular diagnostics and possible targets for personalized therapies. Expert Rev. Mol. Diagn. *15*, 1201–1210.

Porter, E.G., and Dykhuizen, E.C. (2017). Individual bromodomains of polybromo-1 contribute to chromatin association and tumor suppression in clear cell renal carcinoma. J. Biol. Chem. *292*, 2601–2610.

Rawson, R.B. (2013). The site-2 protease. Biochim. Biophys. Acta *1828*, 2801–2807.

Rössler, O.G., and Thiel, G. (2017). Specificity of stress-responsive transcription factors Nrf2, ATF4, and AP-1. J. Cell. Biochem. *118*, 127–140.

Roupé, K.M., Veerla, S., Olson, J., Stone, E.L., Sørensen, O.E., Hedrick, S.M., and Nizet, V. (2014). Transcription factor binding site analysis identifies FOXO transcription factors as regulators of the cutaneous wound healing process. PLoS One *9*, e89274.

Sato, Y., Yoshizato, T., Shiraishi, Y., Maekawa, S., Okuno, Y., Kamura, T., Shimamura, T., Sato-Otsubo, A., Nagae, G., Suzuki, H., et al. (2013). Integrated molecular analysis of clear-cell renal cell carcinoma. Nat. Genet. *45*, 860–867.

Schram, A.W., Baas, R., Jansen, P.W.T.C., Riss, A., Tora, L., Vermeulen, M., and Timmers, H.T.M. (2013). A dual role for SAGA-associated factor *29* (SGF29) in ER stress survival by coordination of both histone H3 acetylation and histone H3 lysine-4 trimethylation. PLoS One *8*, e70035.

Shain, A.H., and Pollack, J.R. (2013). The spectrum of SWI/SNF mutations, ubiquitous in human cancers. PLoS One *8*, e55119.

Shen, C., Beroukhim, R., Schumacher, S.E., Zhou, J., Chang, M., Signoretti, S., and Kaelin, W.G. (2011). Genetic and functional studies implicate HIF1α as a 14q kidney cancer suppressor gene. Cancer Discov. *1*, 222–235.

Shu, X.S., Zhao, Y., Sun, Y., Zhong, L., Cheng, Y., Zhang, Y., Ning, K., Tao, Q., Wang, Y., and Ying, Y. (2017). PBRM1 restricts the basal activity of innate immune system through repressing RIG-I-like receptor signaling and is a potential prognostic biomarker for colon cancer. J. Pathol. *244*, 36–48.

Sizemore, G.M., Pitarresi, J.R., Balakrishnan, S., and Ostrowski, M.C. (2017). The ETS family of oncogenic transcription factors in solid tumours. Nat. Rev. Cancer *17*, 337–351.

Soule, H.D., Maloney, T.M., Wolman, S.R., Peterson, W.D., Brenz, R., McGrath, C.M., Russo, J., Pauley, R.J., Jones, R.F., and Brooks, S.C. (1990). Isolation and characterization of a spontaneously immortalized human breast epithelial cell line, MCF-10. Cancer Res. *50*, 6075–6086.

Suter, M.A., Chen, A., Burdine, M.S., Choudhury, M., Harris, R.A., Lane, R.H., Friedman, J.E., Grove, K.L., Tackett, A.J., and Aagaard, K.M. (2012). A maternal high-fat diet modulates fetal SIRT1 histone and protein deacetylase activity in nonhuman primates. FASEB J. *26*, 5106–5114.

Tatarskiy, V.V., Simonov, Y.P., Shcherbinin, D.S., Brechalov, A.V., Georgieva, S.G., and Soshnikova, N.V. (2017). Stability of the PHF10 subunit of PBAF signature module is regulated by phosphorylation: role of β-TrCP. Sci. Rep. *7*, 5645.

Tiwari, N., Meyer-Schaller, N., Arnold, P., Antoniadis, H., Pachkov, M., van Nimwegen, E., and Christofori, G. (2013). Klf4 is a transcriptional regulator of genes critical for EMT, including Jnk1 (Mapk8). PLoS One *8*, e57329.

Varela, I., Tarpey, P., Raine, K., Huang, D., Ong, C.K., Stephens, P., Davies, H., Jones, D., Lin, M.-L., Teague, J., et al. (2011). Exome sequencing identifies frequent mutation of the SWI/SNF complex gene PBRM1 in renal carcinoma. Nature *469*, 539–542.

Wang, Z., Zhai, W., Richardson, J.A., Olson, E.N., Meneses, J.J., Firpo, M.T., Kang, C., Skarnes, W.C., and Tjian, R. (2004). Polybromo protein BAF180 functions in mammalian cardiac chamber maturation. Gene Dev. *18*, 3106–3116.

Wang, Y., Kallgren, S.P., Reddy, B.D., Kuntz, K., López-Maury, L., Thompson, J., Watt, S., Ma, C., Hou, H., Shi, Y., et al. (2012). Histone H3 lysine 14 acetylation is required for activation of a DNA damage checkpoint in fission yeast. J. Biol. Chem. *287*, 4386–4393.

Wang, Y., Zhou, Y., and Graves, D.T. (2014). FOXO transcription factors: their clinical significance and regulation. Biomed. Res. Int. *2014*, 1–13.

Xia, W., Nagase, S., Montia, A.G., Kalachikov, S.M., Keniry, M., Su, T., Memeo, L., Hibshoosh, H., and Parsons, R. (2008). BAF180 is a critical regulator of p21 induction and a tumor suppressor mutated in breast cancer. Cancer Res. *68*, 1667–1674.

Xue, Y., Canman, J.C., Lee, C.S., Nie, Z., Yang, D., Moreno, G.T., Young, M.K., Salmon, E.D., and Wang, W. (2000). The human SWI/SNF-B chromatin-remodeling complex is related to yeast rsc and localizes at kinetochores of mitotic chromosomes. Proc. Natl. Acad. Sci. U S A *97*, 13015–13020.

Yu, T., Chen, X., Zhang, W., Li, J., Xu, R., Wang, T.C., Ai, W., and Liu, C. (2012). Krüppel-like factor 4 regulates intestinal epithelial cell morphology and polarity. PLoS One *7*, e32492.

ISCI, Volume *15*

Supplemental Information

PBRM1 Regulates Stress Response in Epithelial Cells

Elizabeth G. Porter, Alisha Dhiman, Basudev Chowdhury, Benjamin C. Carter, Hang Lin, Jane C. Stewart, Majid Kazemian, Michael K. Wendt, and Emily C. Dykhuizen

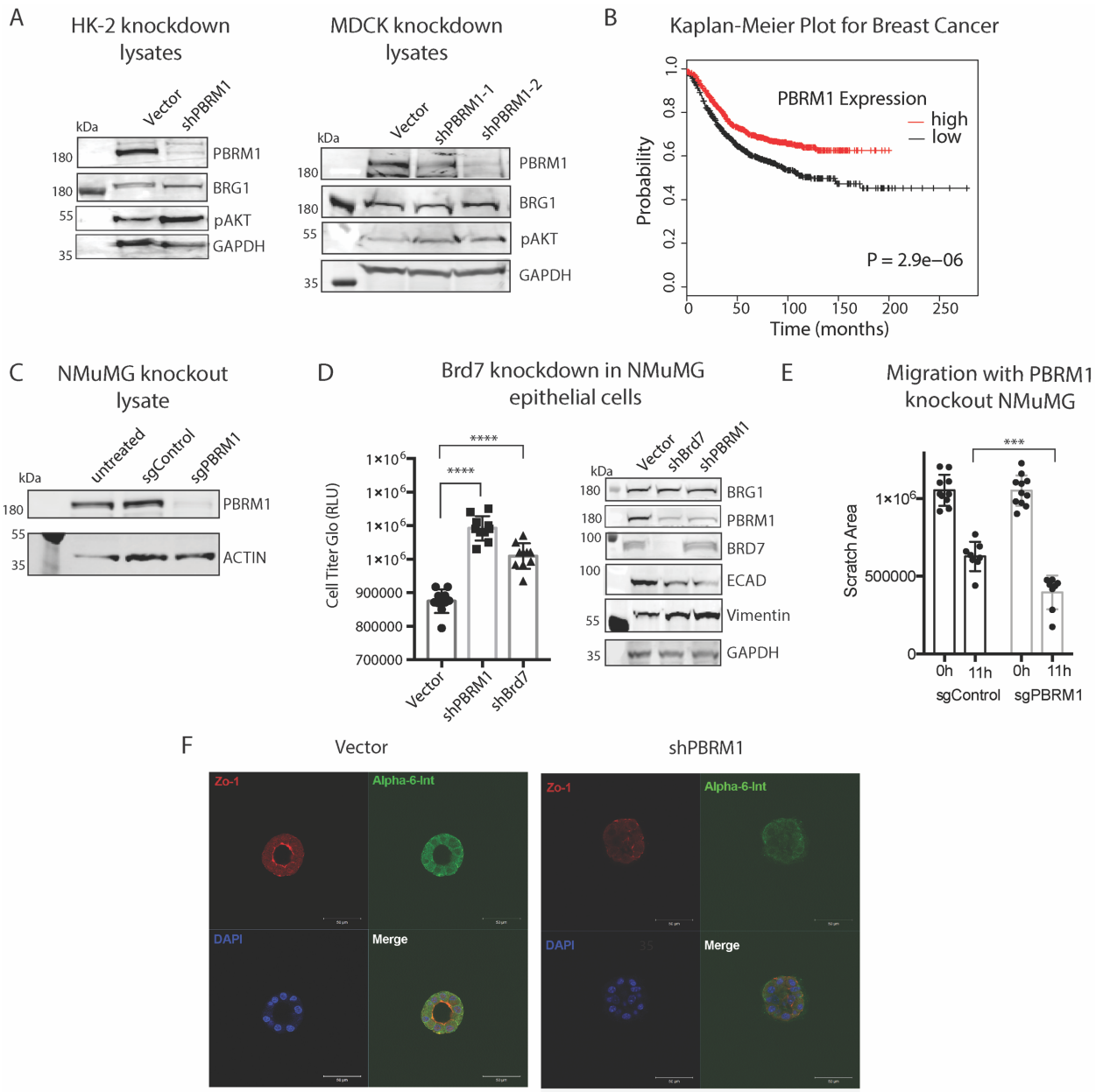

S1: Knockdown of PBRM1 in normal epithelium promotes growth and a loss of epithelial cell maintenance. Related to Figure 1. **A.** Immunoblots of whole cell lysates of epithelial cell lines HK-2 and MDCK with PBRM1 knockdown. **B.** Microarray analysis of breast cancer patients and PBRM1 expression in tumors predicts survival. **C.** Immunoblots of whole cell lysates of epithelial cell line NMuMG with PBRM1 knockout. **D.** NMuMG cells with PBRM1 or BRD7 knockdown were counted after 72h growth and presented as mean ± SD. n = 10. Immunoblot analysis of whole cell lysates from NMuMG cells indicates that PBRM1 or BRD7 knockdown results in decreased E-cadherin expression and increased vimentin expression. **E.** Migration differences between NMuMG control and PBRM1 knockout lines at 0h and 11h. **F.** Representative image of acini from Fig 1E, analyzed using immunofluorescence staining with anti-ZO1 (red) and anti-alpha-6-integrin (green). Nuclei (blue) were visualized by DAPI. *=p <0.05, ** = p <0.01, *** = p < 0.001, **** = p < 0.0001 (paired Student's t test). ns, not significant. Error bars represent S.D

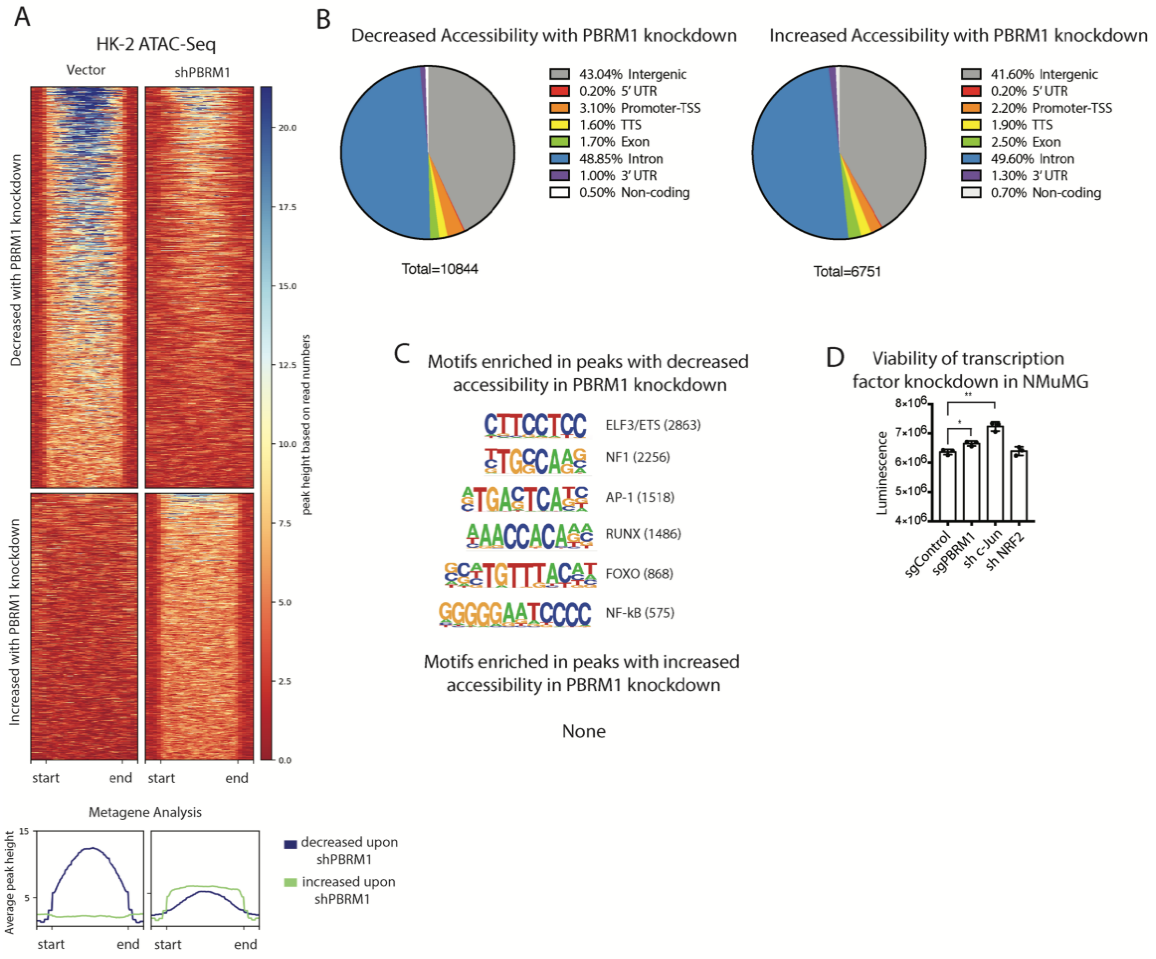

S2: PBRM1 is predicted to cooperate with transcription factors involved in response to stress Related to Figure 2. **A.** Heat maps and metagene plots of regions identified as differentially accessible upon PBRM1 knockdown by ATAC-Seq analysis of HK-2 cells. Regions of at least 1.5-fold differential accessibility were calculated between pooled samples of three biological replicates. **B.** Genomic elements associated with the differentially accessible peaks. The overall distribution was calculated as a percentage of the total differentially accessible regions for each condition. **C.** Motif analysis was performed using HOMER for the differentially accessible peaks. Statistically significant motifs were identified based on relative enrichment over genomic areas with similar AT content. **D.** NMuMG sgcontrol, sgPBRM1, shc-JUN and shNRF2 were cultured and counted after 48h growth. *=p <0.05, ** = p <0.01, *** = p < 0.001, **** = p < 0.0001 (paired Student's t test). Error bars represent S.D. n=3.

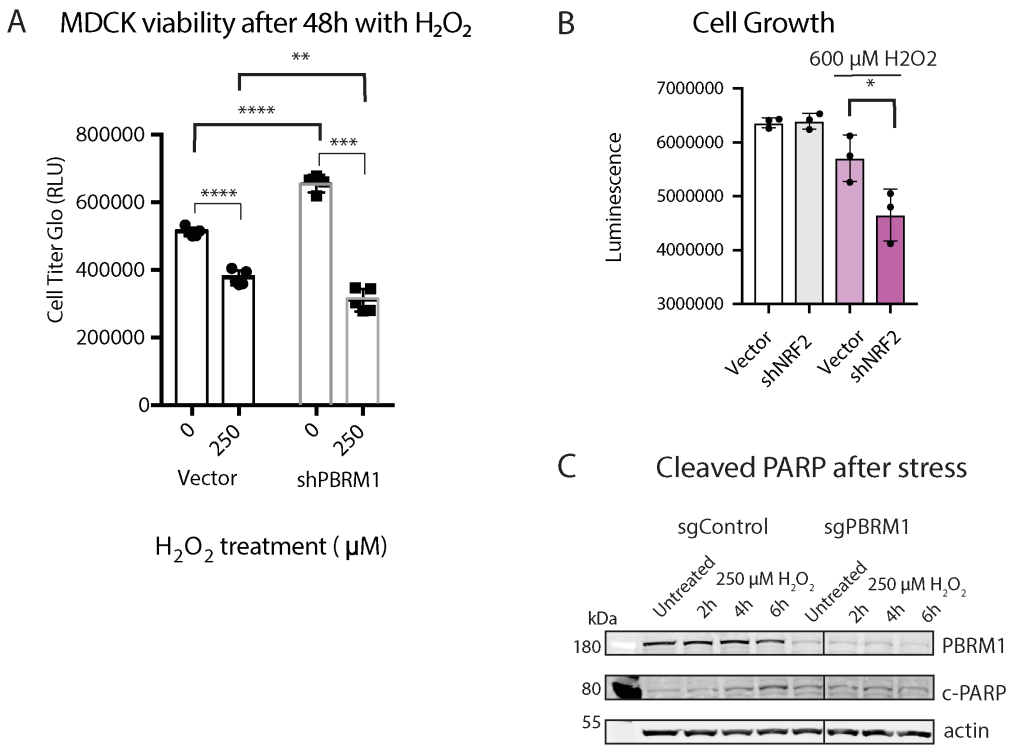

S3: PBRM1 expression is cytoprotective under high stress conditions. Related to Figure 4. **A**. MDCK cells were cultured in normal cell media or 250 µM H_2O_2 for 48 h and luminescence was measured using CellTiter-Glo® assay system and data presented as mean ± SD. n = 4. **B.** NMuMG cells were cultured in normal cell media or 600 µM H_2O_2 for 5 h and luminescence was measured. Data presented as mean ± SD. n = 3. **C.** Immunoblots of whole cell lysates from NMuMG cells treated with 250 µM H_2O_2 for 2h, 4h or 6h. All lanes are from same blot with one irrelevant lane spliced out. *=p <0.05, ** = p <0.01, *** = p < 0.001, **** = p < 0.0001 (paired Student's t test). ns, not significant. Error bars represent S.D.

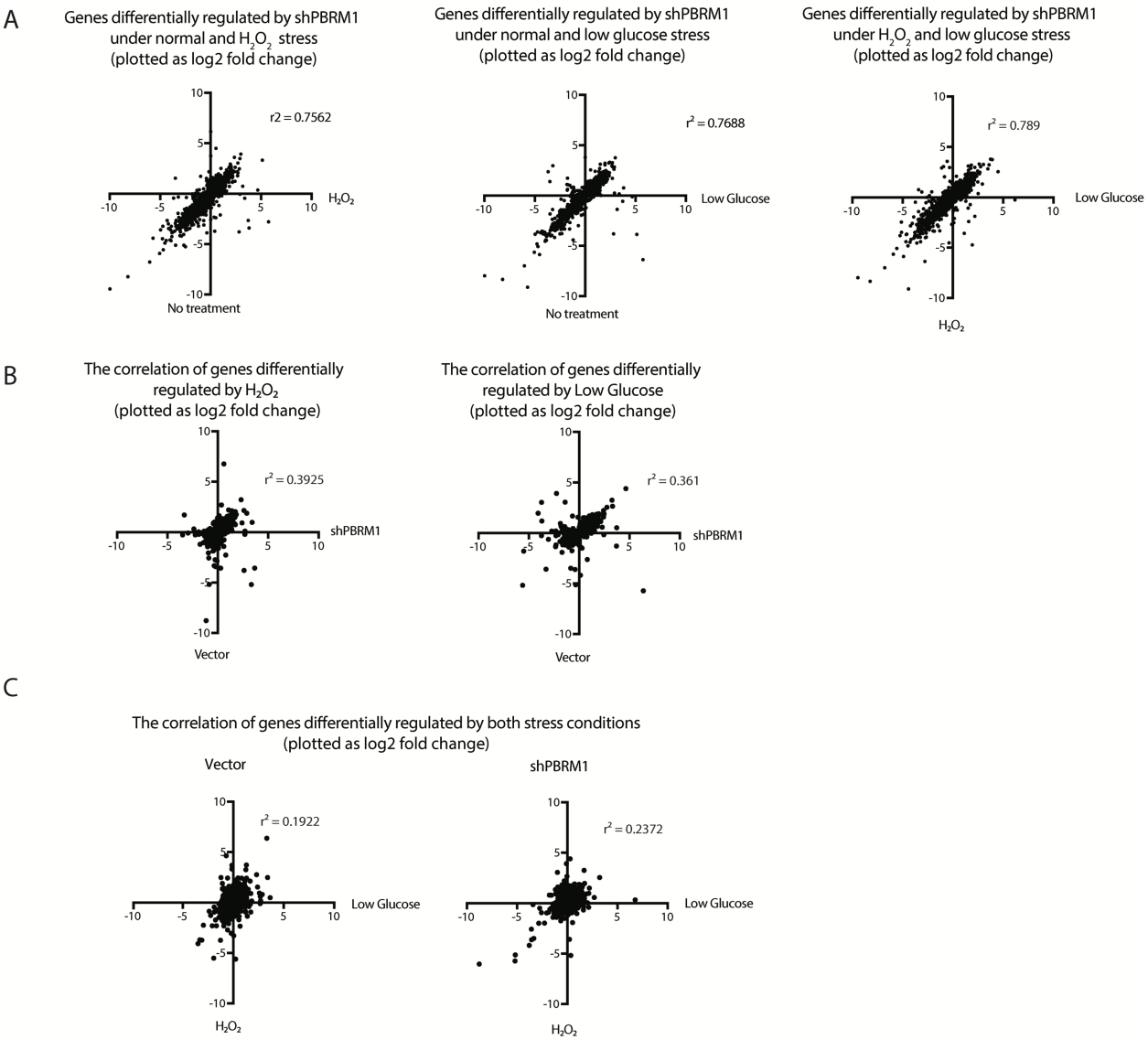

S4: PBRM1-regulated transcriptional effects under cellular stress conditions. Related to Figure 5 and Table 1. **A**. Each data point represents the log2 fold change expression value of a single gene, Left and Center plots- *x axis*: differential expression in H_2O_2 treated cells (left) or low glucose treated cells (center) upon shPBRM1, *y axis*: differential expression in normal cell culture conditions upon shPBRM1 (left and center); Right plot- *x axis:* differential expression under low glucose stress, *y axis:* differential expression under H_2O_2 stress. The degree of correlation was calculated using all differentially expressed genes. **B**. Each data point represents the log2 fold change expression value of a single gene upon 2h H_2O_2 treatment (left) or 6h low glucose treatment (right), *x axis*: differential expression in shPBRM1, *y axis*: differential expression in vector control cells. The degree of correlation was calculated using all differentially expressed genes. **C.** Each data point represents the log2 fold change expression value of a single gene upon 2h H_2O_2 treatment (y axis) or 6h low glucose treatment (x axis) of vector control cells (left) or shPBRM1 cells (right).

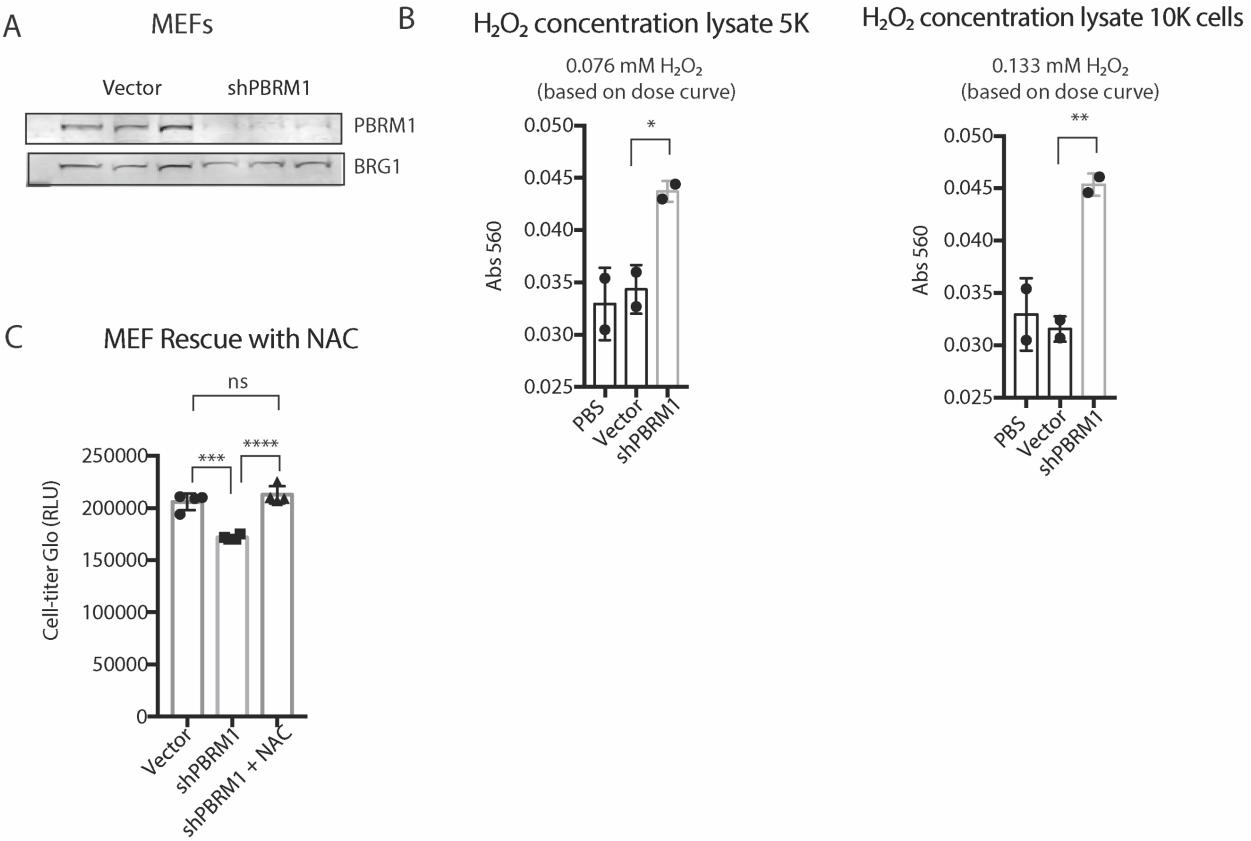

S5: PBRM1 has cell-type specific roles on viability. Related to Figure 6. **A**. PBRM1 knockdown in MEFs was analyzed using immunoblot analysis of nuclear lysates. **B**. Hydrogen peroxide levels were quantitated in MEFs using Amplex® Red Hydrogen Peroxide/Peroxidase Assay Kit. Whole cell lysates were generated from the indicated number of cells in 50 µL RIPA. **C**. MEFs were cultured for 3 days in normal media or media supplemented with 500 µM NAC. Luminescence was measured using CellTiter-Glo® assay system and data presented as mean ± SD. n = 4. *=p <0.05, ** = p <0.01, *** = p < 0.001, **** = p < 0.0001 (paired Student's t test). ns, not significant. Error bars represent S.D.

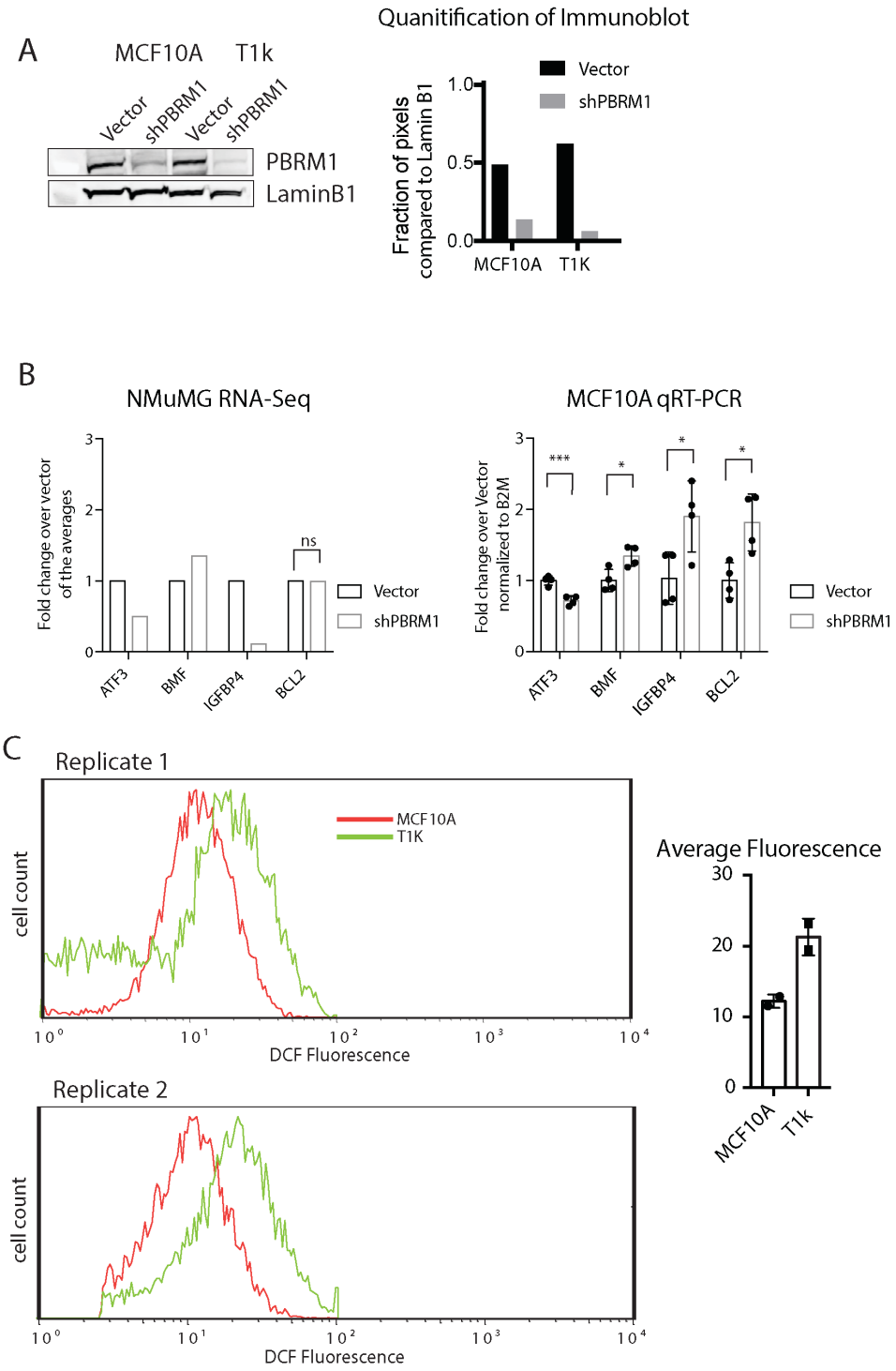

S6: PBRM1 has cell-type specific roles on viability. Related to Figure 6. **A.** PBRM1 knockdown in MCF10A and MCF10A-T1k cell lines was analyzed using immunoblot analysis of nuclear lysates. Quantification indicates the intensity of PBRM1 staining over LaminB1. **B.** Comparison of the expression changes of ATF3, BMF, IGFBP4 and BCL2 in PBRM1 knockdown in mouse mammary epithelial cells (NMuMG: RNA-seq) with human mammary epithelial cells (MCF10A: qPCR). **C.** ROS levels for MCF10A and MCF10A-T1k cells were determined using H_2-DCFDA by flow cytometry. *=p <0.05, ** = p <0.01, *** = p < 0.001, **** = p < 0.0001 (paired Student's t test). ns, not significant. Error bars represent S.D.

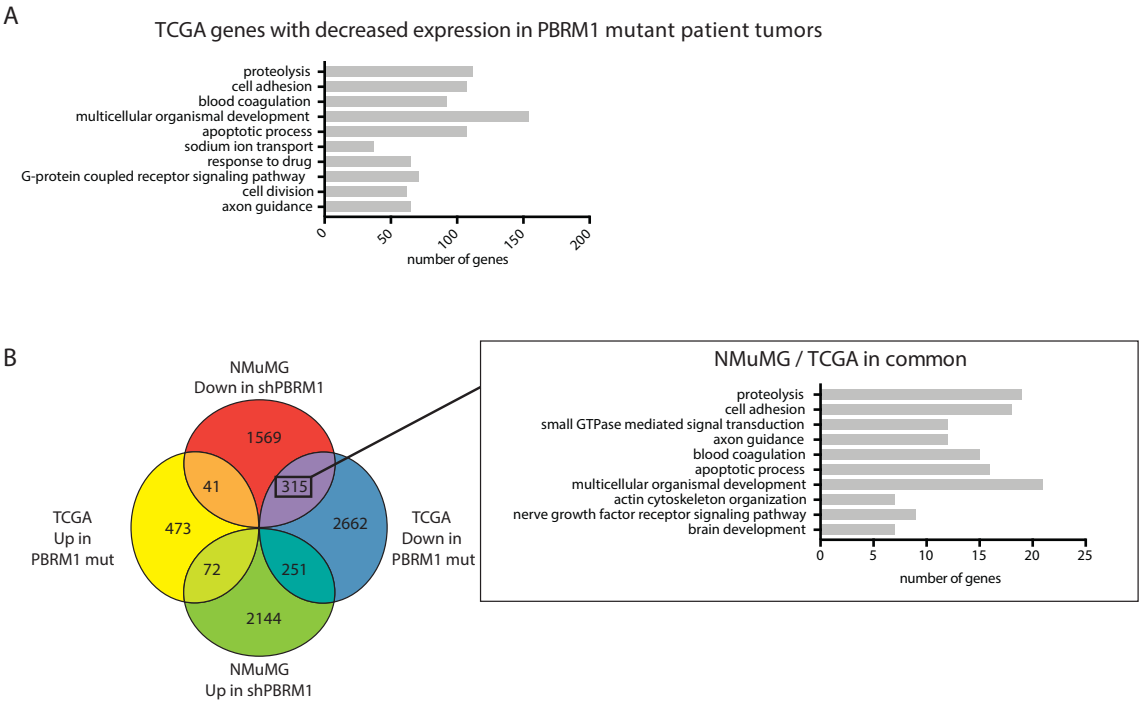

S7: Pathways deregulated upon PBRM1 knockdown in NMuMG cells correlate with TCGA patient dataset. Related to Figure 7. **A**. Summary of genes with decreased expression in renal clear cell carcinoma patients with PBRM1 mutations from The Cancer Genome Atlas (TCGA). **B.** Overlap of differentially regulated genes in NMuMG cells and TCGA patient data. Summary of genes with decreased expression in both NMuMG shPBRM1 and patients with PBRM1 mutations.

TRANSPARENT METHODS

Cell culture

HK-2 were purchased from ATCC and used within 6 months of purchase and 15 passages. Cells were cultured in RPMI (Corning Mediatech) supplemented with 10% fetal bovine serum (J R Scientific), 1% antibiotics (100 units/ml penicillin and 100 g/ml streptomycin; Corning Mediatech), and 1% L-glutamine (Corning Mediatech) at 37 °C in a humidified atmosphere in a 5% CO_2 incubator.

MEF cells were derived from E13.5 day embryos harvested from pregnant 129 mice. Heads and organs were removed and the rest of the embryo was dissociated in trypsin and DNAseI and cultured for 2 passages before performing knockdowns. Cells were cultured in DMEM (Corning Mediatech) supplemented with 10% fetal bovine serum (J R Scientific), 1% antibiotics (100 units/ml penicillin and 100g/ml streptomycin; Corning Mediatech), 1% nonessential amino acids (Corning Mediatech), 1% L-glutamine (Corning Mediatech) and 0.1% β-mercaptoethanol (Gibco, Thermo Scientific) at 37 °C in a humidified atmosphere in a 5% CO_2 incubator.

MCF10A cells were authenticated by STR DNA profiling at Bio-Synthesis (Lewisville, TX) and cultured in 1:1 DMEM (Corning Mediatech) and F12 (Corning Mediatech) supplemented with 29 mM Hepes (Amresco, LLC), 10 mM Sodium Bicarbonate (Macron), 5% Horse serum (Sigma), 10 µg/mL Insulin (Sigma), 10 ng/mL Epidermal Growth Factor (EGF) (Gold Biotechnology), 0.5 µg/mL hydrocortisone (Sigma), 100 ng/mL cholera toxin (Sigma), and 1% antibiotics (100 units/ml penicillin and 100 g/ml streptomycin; Corning Mediatech) at 37 °C in a humidified atmosphere in a 5% CO_2 incubator.

MCF10A T1K were authenticated by STR DNA profiling at Bio-Synthesis (Lewisville, TX) and cultured in DMEM (Corning Mediatech) supplemented with 10% fetal bovine serum (J R Scientific) 1% L-glutamine (Corning Mediatech), 1% antibiotics (100 units/ml penicillin and 100 g/ml streptomycin; Corning Mediatech), and 1% Sodium Pyruvate (Corning Mediatech) at 37 °C in a humidified atmosphere in a 5% CO_2 incubator.

NMuMG cells were purchased from ATCC and used within 6 months of purchase and 15 passages. Cells were grown in DMEM (Corning Mediatech) supplemented with 10% fetal bovine serum (J R Scientific), 10 µg/mL Insulin (Sigma), 1% L-glutamine (Corning Mediatech), 1% antibiotics (100 units/ml penicillin and 100 g/ml streptomycin; Corning Mediatech), and 1% Sodium Pyruvate (Corning Mediatech) at 37 °C in a humidified atmosphere in a 5% CO_2 incubator.

MDCK cells were purchased from ATCC and used within 6 months of purchase and 10 passages. Cells were cultured in DMEM (Corning Mediatech) supplemented with 10% fetal bovine serum (J R Scientific), 1% L-glutamine (Corning Mediatech), 1% antibiotics (100 units/ml penicillin and 100 g/ml streptomycin; Corning Mediatech), 1% nonessential amino acids (Corning Mediatech), 10 mM Hepes (HyClone) and 1% Sodium Pyruvate (Corning Mediatech), at 37 °C in a humidified atmosphere in a 5% CO_2 incubator.

Caki2 cells were originally purchased from ATCC and subsequently authenticated by STR DNA profiling at Bio-Synthesis (Lewisville, TX). Cells were grown in McCoy's 5A medium (Corning Mediatech) supplemented with 10% fetal bovine serum (J R Scientific), 1% antibiotics (100 units/ml penicillin and 100 g/ml streptomycin; Corning Mediatech), 1% nonessential amino acids (Corning Mediatech), and 1% L-glutamine (Corning Mediatech) at 37 °C in a humidified atmosphere in a 5% CO2 incubator. Caki2 Fuw and Caki2 Fuw+PBRM1 cells were cultured in the presence of doxycycline (1 µg/ml final concentration).

All the media were supplemented with 1:10,000 dilution of Plasmocin™ (InvivoGen).

Cell culture and treatments

Cells were seeded 24-72 h before treatment such that they were 50-80 % confluent at the time of experiment. For hydrogen peroxide treatment, indicated concentrations of freshly prepared hydrogen peroxide were added to the treatment groups for the indicated time periods in their regular media. For glucose starvation studies, the regular media was replaced with glucose free DMEM media (Corning Mediatech) or reduced glucose media for the indicated time periods. Following the completion of

treatment, cells were washed once with PBS, harvested by trypsinization and either processed immediately or flash frozen and stored at -80 ºC for future use.

Generation of cell lines

Knockdown was performed using shRNA-mediated knockdown with lentiviral construct pLKO.1. The shRNA constructs contain the following mature antisense sequences:
Human PBRM1: (TRCN0000015994) TTTGTAGATCAAAGACTCCGG
Mouse PBRM1: (TRCN0000081820) TTCTAGGTTGTATGCCTGTCG
Mouse Brd7 Clone ID: (TRCN0000030015) ATAATCATGGAGTAGCCAGGC
Mouse Brg1: (TRCN0000071386) TTCTCAATAATGTGTCGGGCG
Mouse Arid1a: (TRCN0000071395, Origene TG517733) ATTGTAGGTCATGTCATTTCG
Canine PBRM1-1: ACATCATCATACTCTTCCA
Canine PBRM1-2: ACCAACAGCCATACAACCA
c-Jun (TRCN0000042695): GCTTAAGCAGAAAGTCATGAAC
NRF2 (TRCN0000054658):GCCAAAGCTAGTATAGCAATAA

Caki2 FUW vector and Caki2 FUW PBRM1 as described in Chowdhury et al. 2016.

Short guide RNA for mouse PBRM1 (sgPBRM1) was designed using the MIT CRISPR tool (http://crispr.mit.edu/) and the control sgRNA (sgControl) was taken from Alpsoy and Dykhuizen et al. 2018 (Alpsoy and Dykhuizen, 2018).

Mouse sgControl: GTAGCGAACGTGTCCGGCGT

Mouse sgPBRM1: TTCATCCTTATAGTCTCGGA

The sgRNA were ordered as single strand oligos, annealed and cloned into vector PX459 (pSpCas9(BB)-2A-Puro (PX459) V2.0 was a gift from Feng Zhang, Addgene plasmid # 62988). The constructs were introduced into NMuMG cells by transient transfection using Lipofectamine 3000 (Invitrogen). After 48 h of transfection, selection using puromycin (0.6 µg/ml) was done for 48 h. The efficiency of knockout constructs was confirmed by immunoblotting.

Lentiviral Infection
HEK293T cells were transfected with knockdown and knockout lentivirus constructs along with packaging vectors pMD2.G and psPAX2. After 48 h, the supernatant was collected and concentrated by ultracentrifugation (17,300 rpm for 2 h) and resuspended in 200 µl of PBS. Cells were infected with concentrated virus using spinfection (1500 rpm in swing bucket centrifuge for 1 h). Fresh medium was added 16 h after infection, and cells were allowed to recover for 24 h before selection. Cells were selected for 2 weeks with puromycin (0.6 µg/ml) (Sigma-Aldrich) and hygromycin (200 µg/ml) where applicable (Corning Mediatech). Caki2 cells were cultured with 2 µg/ml doxycycline (EMD Chemicals) for 72 h prior to experiments to induce protein expression which was confirmed by immunoblotting. The efficiency of all constructs was confirmed by immunoblotting.

3D culture
Cells were embedded between 2 layers of Cultrex® Basement Membrane Extract (BME) (R&D Systems) on 8-well Chamber Slide. Wells were pre-coated with BME (200 µl/well) to allow polymerization at 37°C for 15 minutes. Cells were then seeded at 20,000 cells/well density. After attachment (30 minutes at 37°C), cells were covered with a second layer of BME/culture medium (1:19, 5%) to polymerize overnight at 37°C. Cells were incubated for 10 days, and the medium was replenished every 3 days. At the end of incubation, cells were fixed and subjected to immunofluorescence analysis.

Immunofluorescence staining
Cells were washed twice with ice-cold PBS, added 2-3 volumes of ice-cold PBS-EDTA and shaken on ice for 15-30 minutes. BME was detached from the bottom of culture surface by gently scraping the bottom with a pipette tip. The solution was transferred to a conical tube and gently shaken on ice for 15-30 minutes. When BME was dissolved completely, the solution was centrifuged at 120g for 1-2 minutes. The supernatant was carefully aspirated, and cells were gently resuspended in the remaining supernatant.

Pipetted approximated 15 µl of the cell suspension onto a glass bottom dish, allowed cells to settle and adhere to the glass. Cells were fixed using formalin for 20 minutes at room temperature (RT). Next, cells were permeabilized with 0.5% Triton X-100 in PBS for 5 minutes at RT and washed 3 times with 100 mM glycine in PBS at RT. Fixed cells were blocked for 1.5 hours with 10% goat serum. Cells were incubated overnight at 4°C with primary antibodies. The primary antibodies used were as follows: rat anti–α_6-integrin (Millipore; 1:100 in 0.2% Triton X-100, 0.1% BSA, 0.05% Tween 20 in PBS) and rabbit anti–Zo-1 (Invitrogen, 1:100 in 0.2% Triton X-100, 0.1% BSA, 0.05% Tween 20 in PBS). Cells were incubated with secondary antibody for 1 hour, followed by 3 washes at RT. Secondary antibodies were as follows: FITC goat anti-rat and Biotin-SP-conjugated AffiniPure goat anti-rabbit (Jackson ImmunoResearch). Cells were incubated with Texas Red Avidin D (Vector) for 1hour. Cell nuclei were counterstained with DAPI for 10 minutes and washed 3 times with PBS. Cells were incubated in PBS and imaged by confocal microscopy.

Confocal microscopy
Confocal laser scanning microscopy experiments were conducted using the Zeiss LSM 880 Upright Confocal.

TopFlash Reporter Assay
NMuMG cells were transfected with 10:1 ratio of M50 Super 8x TopFlash (Addgene 12456) to pcDNA3.1.CMV-renilla-Neo. The cells were transfected using Lipofectamine with 3:1 ratio of total DNA to lipofectamine reagent. After 24 h, the cells were trypsinized and 20,000 cells/well were plated in 96-well white tissue culture treated plates. After an additional 24 h of growth, the firefly and renilla luciferase levels were measured using the Dual Glo® assay system (Promega).

Annevin V Apoptosis detection in NMuMG cells
NMuMG cells were seeded at a density of ~ 1.5 X 10^6 cells/60mm dish and cultured for 24 h. The cells were then given treatments of 200 µM H_2O_2 in media for 0-4 h, followed by cell harvesting using Accutase (Innovative cell technologies) and apoptosis detection using the FITC Annexin V apoptosis detection kit (BD Pharmingen, Cat. # 556547) as per the manufacturer's instructions. The cells were immediately analyzed by flow cytometry using the Guava EasyCyte Benchtop Flow Cytometer (Millipore Sigma). The results were analyzed using FlowJo software.

Immunoblotting
Cells were given treatments as described before for the indicated time periods, followed by cell harvesting by trypsinization. Whole cell extracts were prepared by dissolving the cell pellets in RIPA buffer (50 mM Tris (pH 8.0), 150 mM NaCl, 0.1% SDS, 0.5% Na Deoxycholate, 1% NP-40) supplemented with freshly added PMSF, aprotinin, leupeptin and pepstatin, and incubation for 30 min at 4 °C. The lysates were centrifuged at 13000 x g for 30 min at 4 °C and the supernatants were preserved. Protein concentration estimations for the supernatants were done using BCA protein assay kit (Pierce Biotechnology) with BSA as standard and whole cell extracts were run on a 4-12 % bis-tris gradient protein gel, transferred to PVDF membrane and probed with primary antibodies in 5% BSA at 4 °C for 16 h.

Antibodies
Cleaved PARP (Asp214) (7C9) (Mouse specific) Cell Signaling #9548
Cleaved PARP (Asp214) (Human Specific) Cell Signaling #9541
PBRM1 (Bethyl Laboratories-PBRM1 Antibody, #A301-591A)
β-actin (Santa Cruz Biotechnology, #sc-47778)
BRG1 (G-7) Santa Cruz sc-17796
BRD7 Bethyl A302-304A
Vimentin BD Biosciences 550513
E-Cadherin BD Biosciences 610182
GAPDH (6C5) (Santa Cruz sc-32233)
LaminB (A-11) sc-377000
Phospho-Akt (Ser473) (D9E) XP® (Cell Signaling #4060)

Migration assay

NMuMG cells were seeded at a density of ~ 1.5 X 10^6 cells/well in a 6-well plate and cultured for 24 h, after which scratches were made in each well. The migration of cells was followed at regular intervals as indicated.

H_2-DCFDA staining for intracellular ROS using flow cytometry
NMuMG cells were seeded at a density of ~ 2 x 10^6 cells/60mm dish and Caki2 cells were seeded at a density of ~ 3 X 10^6 cells/60mm dish. The cells were cultured for 48 h, harvested by trypsinization, washed once with PBS and stained for intracellular ROS by incubation with freshly prepared 10 µM H2-DCFDA (Invitrogen, Cat. # D399) in PBS for 30 min at 37 °C in dark. Following the incubation, the cells were centrifuged at 250 x g for 5 min, resuspended in PBS and immediately analyzed by flow cytometry. The results were analyzed using FlowJo software.

Stress treatments and H_2-DCFDA staining using microplate reader
NMuMG cells were seeded at a density of 6.0 x 10^4 cells/well and Caki2 cells were seeded at a density of 2.5X10^4 cells/well in a 96-well black tissue culture plates. The cells were cultured for 24 h, following which they were subjected to the following stress conditions: H_2O_2 treatment (0-200 µM for NMuMG and 0-800 µM for Caki2) for 1h followed by 10 min recovery in PBS, glucose starvation by culturing in various glucose concentrations for 16 h for NMuMG and culturing in glucose free media for the indicated time periods for Caki2, CoCl2 treatment (0-250µM) for 24h or doxorubicin treatment (0-10 µM) for 24h. At the end of the treatments, cells were washed once with PBS, and stained with freshly prepared 10 µM H_2-DCFDA (Invitrogen, Cat. # D399) in PBS for 30 min at 37 °C in dark. Cells were washed again 2x with PBS and fluorescence measurements were taken using a microplate reader at excitation/emission wavelengths of 485/530 nm. Unstained cells were used as the negative controls.

H_2O_2 detection assay
H_2O_2 levels were measured using Amplex® Red Hydrogen Peroxide/Peroxidase Assay kit (Invitrogen). The H_2O_2 levels were determined from whole cell lysates (in RIPA) according to manufacturer's instruction. The concentration of H_2O_2 was determined for lysates generated from 5,000 and 10,000 cells in 50 µL by plotting fluorescence levels against experimentally determined dose curves.

Viability assays using CellTiter-Glo®
Cells were plated in 96-well white tissue culture plates and cultured for the indicated time under the indicated conditions. Antioxidant rescue experiments were performed with fresh media daily containing 20 µg/mL Vitamin C or 250 µM N-acetylcysteine (NAC). CellTiter-Glo® assay reagent was added directly to cells as per manufacturer's instructions, incubated for 10 min, and the luminescence was measured on a GloMax® microplate reader.

LDH assays using LDH Cytotoxicity Assay Kit II (Abcam, ab65393)
NMuMG cells were seeded at a density of 6.0 x 10^4 cells/well and Caki2 cells were seeded at a density of 1.0 x 10^4 cells/well in 96-well tissue culture plates. The cells were cultured for 24 h, following which they were subjected to H_2O_2 treatment (0-300 µM for NMuMG) for 6h or 24h and 200 µM H_2O_2 for Caki2 for the indicated time periods. Media was harvested from wells (10 µL) and transferred to a separate 96-well assay plate along with negative control (media alone) and positive control (lysed cells). LDH Reaction Mix (100 µl) was added to each well, mixed and incubated for 30 min at room temperature. The absorbance at 490 nm was measured on the GloMax® microplate reader.

H_2-DCFDA staining for MCF10A and MCF10A-T1K followed by flow cytometry
MCF10A and MCF10A-T1K cells were seeded in 60mm dishes in MCF10A media and cultured for 48 h such that they reach 50-80 % confluency at the day of the experiment. The cells were then harvested using trypsin, washed once using serum-free and phenol red-free media and stained for intracellular ROS with freshly prepared 10 µM H_2-DCFDA in PBS-Glucose (1X PBS supplemented with 25 mM glucose) as described before. The cells were immediately examined by flow cytometry and the results were analyzed using FlowJo software.

RNA-seq

RNA isolation, library construction, sequencing and transcriptome analysis was performed as described in our previous publication (Chowdhury et al. 2016). Sequencing was performed in biological triplicates. RNA-seq of NMuMG epithelial cell lines was performed at the Purdue Genomics Core using Illumina HiSeq technology. The resulting reads were trimmed using Trimmomatic utility (Bolger et al., 2014) and mapped to mm9 using STAR (Dobin et al., 2013) using default parameters. Read counts were obtained using HTSeq-count (Anders et al., 2015) in conjunction with a standard gene annotation files from UCSC (University of California Santa Cruz; http://genome.ucsc.edu) and differential expression was determined using DESeq2 pipeline (Love et al., 2014). Differentially expressed genes were filtered using a false discovery rate threshold of < 0.05 and a fold change threshold of > 1.3-fold relative to the reference sample. Gene ontology and transcription factor prediction analyses were performed using GeneCodis (Nogales-Cadenas et al., 2009) iCisTarget (Herrmann et al., 2012), and ToppCluster (Kaimal et al., 2010). Data sets generated in these experiments are available at the Gene Expression Omnibus under accession number GSE113606.

ATAC-seq

The ATAC-seq protocol originally described (Buenrostro et al., 2015) was adapted as follows for HK2 and NMuMG isogenic lines: 50,000 cells were resuspended in Nuclei Lysis buffer containing 0.05% IGEPAL CA-630, incubated for 5 minutes on ice and centrifuged for 10 minutes at 500xg at 4 °C. Nuclei extraction was confirmed by microscopic inspection and the nuclei pellet was resuspended in transposition master mix. Tagmentation, cleanup of tagmented DNA, and PCR enrichment was performed as per original description. High throughput sequencing was performed by HiSeq2500 using 50 bp paired-end at the Purdue Genomics Core. Sequenced reads were mapped by the Bowtie2 aligner (Ben Langmead et al., 2009) using hg19 or mm10 reference genome, respectively. Reads mapping to the mitochondrial genome were discarded. Bigwig files were generated for visual inspection of tracks using the bamCoverage utility of deepTools (Ramírez et al., 2016). Peaks of differential accessibility were identified using the SICER-df-rb utility (Xu et al., 2014) with a false discovery rate threshold of < 0.05 and a fold change threshold of > 1.5-fold difference in accessibility. Scaled heat maps were generated for the peak regions using the computeMatrix and plotHeatmap utilities of deepTools. Peak regions were analyzed for enrichment of sequence motifs and association with genomic elements using the findMotifs and annotatePeaks utilities of HOMER (Heinz et al., 2010).

qRT-PCR

RNA was isolated from cells using Trizol (Ambion, Thermofisher). Total RNA was converted to cDNA with Verso cDNA Synthesis Kit according to manufacturer's instructions (Thermo Scientific). Real-time PCR was performed using a Bio-Rad CFX Connect Real-Time system and Thermo Scientific Maxima SYBR Green qPCR Master Mix (Thermo Scientific). The results were analyzed using the Pfaffl method (Pfaffl, 2001).

Gene	Forward Primer	Reverse Primer
c-Jun	ACTCGGACCTTCTCACGTC	GGTCGGTGTAGTGGTGATGT
BCL2L1	GACAAGGAGATGCAGGTATTGG	TCCCGTAGAGATCCACAAAAGT
HK2	TGATCGCCTGCTTATTCACGG	AACCGCCTAGAAATCTCCAGA
IL1RL1	ACGCTCGACTTATCCTGTGG	CAGGTCAATTGTTGGACACG
NRF2	GATCCGCCAGCTACTCCCAGGTTG	CAGGGCAAGCGACTCATGGTCATC
HMOX1	GCCGAGAATGCTGAGTTCATG	TGGTACAAGGAAGCCATCACC
NQO1	CGCCTGAGCCCAGATATTGT	GCACTCTCTCAAACCAGCCT
BMF	GTGGCAACATCAAGCAGAGG	CGGTGGAACTGGTCTGCAA
ATF3	CTGCAGAAAGAGTCGGAG	TGAGCCCGGACAATACAC
IGFBP4	CTCTTCCGGTGCTGACCTCT	GGTGCTCCGGTCTCGAAT
BCL2	CTGCACCTGACGCCCTTCACC	CACATGACCCCACCGAACTCAAAGA

TCGA analysis

TCGA data analysis was performed as described in Chowdhury et al. 2016.

Data and software availability

Data sets generated in these experiments are available at the Gene Expression Omnibus under accession number GSE113606.

Supplemental References

Alpsoy, A., Dykhuizen, E.C., 2018. Glioma tumor suppressor candidate region gene 1 (GLTSCR1) and its paralog GLTSCR1-like form SWI/SNF chromatin remodeling subcomplexes. J Biol Chem 293, 3892–3903. doi:10.1074/jbc.RA117.001065

Anders, S., Pyl, P.T., Huber, W., 2015. HTSeq--a Python framework to work with high-throughput sequencing data. Bioinformatics 31, 166–169. doi:10.1093/bioinformatics/btu638

Ben Langmead, Trapnell, C., Pop, M., Salzberg, S.L., 2009. Ultrafast and memory-efficient alignment of short DNA sequences to the human genome. Genome Biol 10, R25. doi:10.1186/gb-2009-10-3-r25

Bolger, A.M., Lohse, M., Usadel, B., 2014. Trimmomatic: a flexible trimmer for Illumina sequence data. Bioinformatics 30, 2114–2120.

Buenrostro, J., Wu, B., Chang, H., Greenleaf, W., 2015. ATAC-seq: A Method for Assaying Chromatin Accessibility Genome-Wide. Current protocols in molecular biology / edited by Frederick M. Ausubel ... [et al.] 109, 21.29.1–21.29.9. doi:10.1002/0471142727.mb2129s109

Dobin, A., Davis, C.A., Schlesinger, F., Drenkow, J., Zaleski, C., Jha, S., Batut, P., Chaisson, M., Gingeras, T.R., 2013. STAR: ultrafast universal RNA-seq aligner. Bioinformatics 29, 15–21.

Heinz, S., Benner, C., Spann, N., Bertolino, E., Lin, Y.C., Laslo, P., Cheng, J.X., Murre, C., Singh, H., Glass, C.K., 2010. Simple combinations of lineage-determining transcription factors prime cis-regulatory elements required for macrophage and B cell identities. Mol Cell 38, 576–589. doi:10.1016/j.molcel.2010.05.004

Herrmann, C., Van de Sande, B., Potier, D., Aerts, S., 2012. i-cisTarget: an integrative genomics method for the prediction of regulatory features and cis-regulatory modules. Nucleic Acids Research 40, e114–e114. doi:10.1093/nar/gks543

Kaimal, V., Bardes, E.E., Tabar, S.C., Jegga, A.G., Aronow, B.J., 2010. ToppCluster: a multiple gene list feature analyzer for comparative enrichment clustering and network-based dissection of biological systems. Nucleic Acids Research 38, W96–W102. doi:10.1093/nar/gkq418

Love, M.I., Huber, W., Anders, S., 2014. Moderated estimation of fold change and dispersion for RNA-seq data with DESeq2. Genome Biol 15, 550. doi:10.1186/s13059-014-0550-8

Nogales-Cadenas, R., Carmona-Saez, P., Vazquez, M., Vicente, C., Yang, X., Tirado, F., Carazo, J.M., Pascual-Montano, A., 2009. GeneCodis: interpreting gene lists through enrichment analysis and integration of diverse biological information. Nucleic Acids Research 37, W317–W322. doi:10.1093/nar/gkp416

Pfaffl, M.W., 2001. A new mathematical model for relative quantification in real-time RT-PCR. Nucleic Acids Research 29, e45.

Ramírez, F., Ryan, D.P., Grüning, B., Bhardwaj, V., Kilpert, F., Richter, A.S., Heyne, S., Dündar, F., Manke, T., 2016. deepTools2: a next generation web server for deep-sequencing data analysis. Nucleic Acids Research 44, W160–W165. doi:10.1093/nar/gkw257

Xu, S., Grullon, S., Ge, K., Peng, W., 2014. Spatial clustering for identification of ChIP-enriched regions (SICER) to map regions of histone methylation patterns in embryonic stem cells. Methods Mol. Biol. 1150, 97–111. doi:10.1007/978-1-4939-0512-6_5